

Global Hybrid Modeling of the Magnetosphere

Yu Lin

Physics Department, Auburn University, AL

In collaboration with Xueyi Wang¹, J. D. Perez¹, San Lu², Lei Cheng¹, Zhifang Guo¹, J. R. Johnson³, Chih-Ping Wang⁴, and Terry Liu⁵

¹Physics Department, Auburn University, AL

²IGPP, UCLA, CA

³Andrews University, MI

⁴Atmospheric and Oceanic Sciences, UCLA, CA

⁵Physics Department, UAF, AK

1. Introduction
2. 3-D global hybrid simulation model
3. Results (1): generation of kinetic Alfvén waves (KAWs) from the magnetotail to the ionosphere associated with fast flows I
4. Results (2): magnetopause reconnection and comparison with MMS observations
5. Results (3): propagation of foreshock transients to the tail
6. Summary

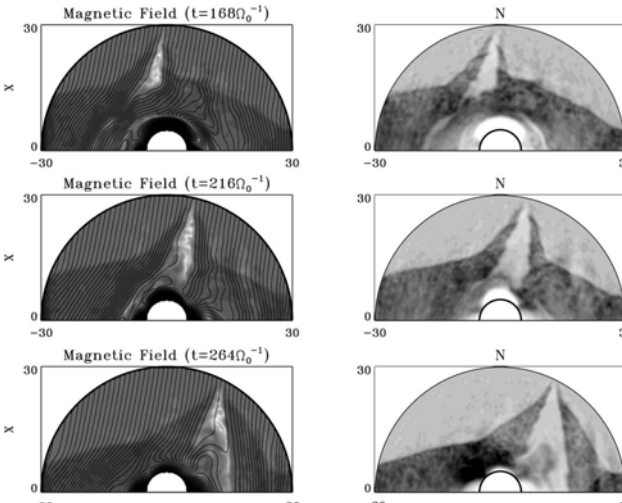


1. Introduction

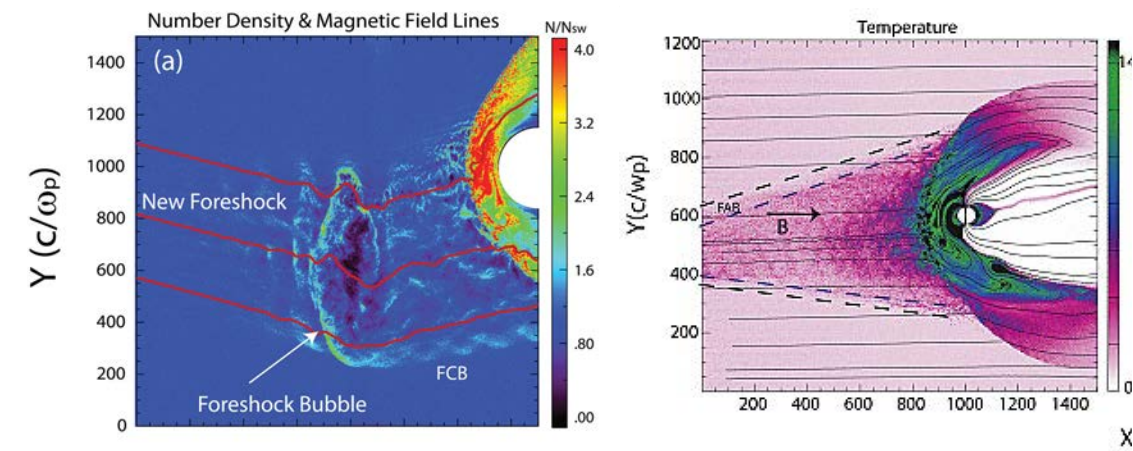
- Ion kinetic physics is important in the structure of collisionless bow shock, magnetopause, and tail plasma sheet (scale length $\sim \rho_i$).
- Ion kinetic physics is important in the global structure and dynamic processes in the solar wind-magnetosphere interaction.
- Hybrid-particle simulation is a first-principles approach to address the ion kinetic physics in the self-consistent electromagnetic field.
- In this talk, I will present 3-D global hybrid simulation results on a few important processes in the magnetosphere.



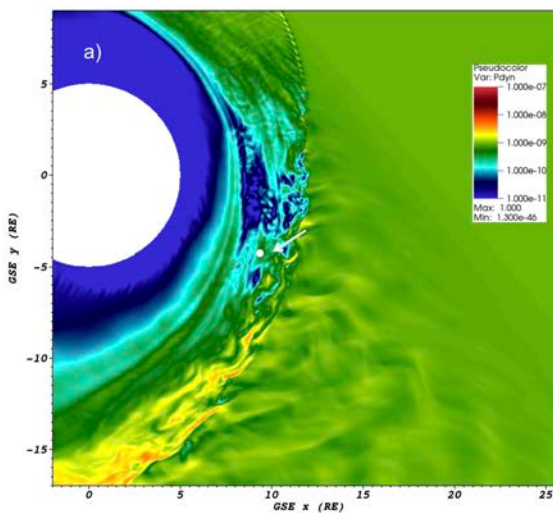
Global hybrid simulations of the dayside foreshock transients



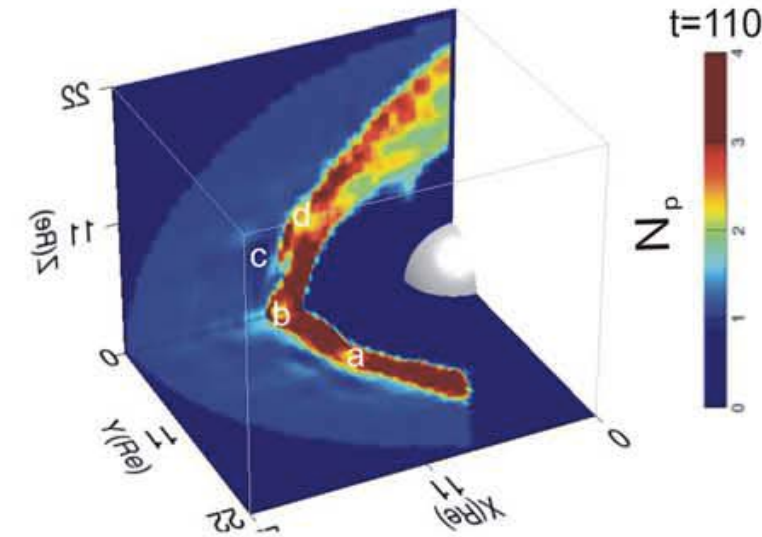
HFA [*Lin*, 2002]



Foreshock bubble [*Omidi+*, 2020]



Magnetosheath jets [*Palmroth+*, 2018]



Magnetopause pressure pulses due to Foreshock cavities [*Lin and Wang, 2005*]

2. ANGE3D: A 3-D Global Hybrid Model

Auburn Global hybrid code in 3-D (ANGE3D) [*Lin et al.*, 2014, 2017] (previously dayside [*Swift*, 1996; *Lin and Wang*, 2005] and nightside [*Swift and Lin*, 2001]).

- Fully kinetic ions; electron fluid; quasi-charge neutrality.
- No electron inertial effects included.
- Cartesian coordinate system: **Simulation domain:**

$$x = -60 \text{ to } 20R_E$$

$$y = -30 \text{ to } 30R_E$$

$$z = -30 \text{ to } 30R_E$$

Inner boundary assumed at $r \approx 3 R_E$.

- Cold ion fluid in $r < 6R_E$ [*Swift*, 1996; *Lin and Wang*, 2005], coexisting with particle ions; fully kinetic ions outside.
- Ad-hoc current-dependent resistivity.
- **Initial setup:** Dipole plus mirror dipole field and IMF/solar wind.

- **Particle and field advance scheme:**

Ions: particle-in-cell (PIC), equation of motion:

$$m_p d\mathbf{v}_p/dt = e(\mathbf{E} + \mathbf{v}_p \times \mathbf{B}) - v m_p (\mathbf{V}_p - \mathbf{V}_e).$$

Electron momentum equation (to calculate \mathbf{E}):

$$\cancel{m_e n d\mathbf{V}_e/dt} = -en(\mathbf{E} + \mathbf{V}_e \times \mathbf{B}) - v n m_p (\mathbf{V}_e - \mathbf{V}_i) - \nabla P_e,$$

Ampere's law:

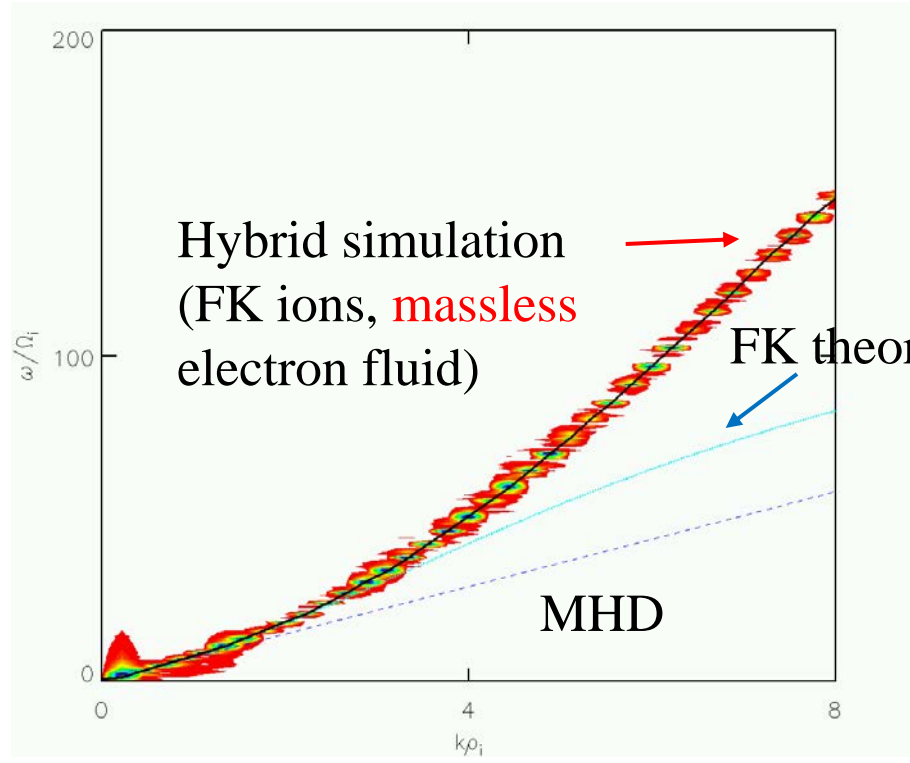
$$\mathbf{V}_e = \mathbf{V}_i - \nabla \times \mathbf{B} / \mu_0 n e,$$

Faraday's law: $\partial \mathbf{B} / \partial t = - \nabla \times \mathbf{E}$.

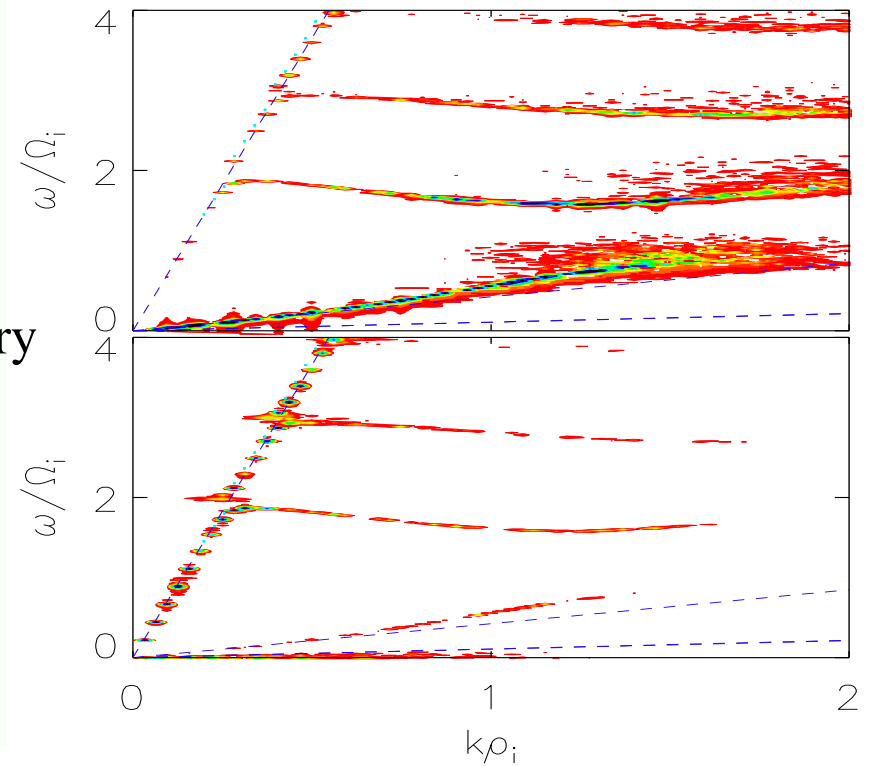
- **Boundary conditions:**
 - (1) Sunward side ($x=20R_E$): solar wind and IMF (fixed or variable); all other sides of outer boundaries: free;
 - (2) Inner boundary ($r \approx 3R_E$): Ionospheric conditions. $J_{||}$ is mapped along field lines as input to the ionospheric potential equation. The potential is then mapped back to the boundary. Use static conductance models ($\Sigma_P = 5$ Siemens, $\Sigma_H = 10$ Siemens).
- **Physics of $\omega \sim \Omega_i$ and $k\rho_i \sim 1$ ($\lambda \sim 6\rho_i$), so grid sizes $\sim \rho_i$ or d_i .**
- Solar wind $d_i = 0.05 - 0.1R_E$.
- Ion FLR effects are resolved with particle time steps Δt much smaller than the gyro-period: $\Delta t = 0.05\Omega_{i0}^{-1}$. Subcycling time steps in the field advance.
- Normalization:
 B -- nT; time -- sec; length -- R_E ; V -- km/s; T – eV; J – mA/cm².
- Scaling factor

Hybrid model resolves physics of $k\rho_i \sim 1$ and $\omega \sim \Omega_i$:

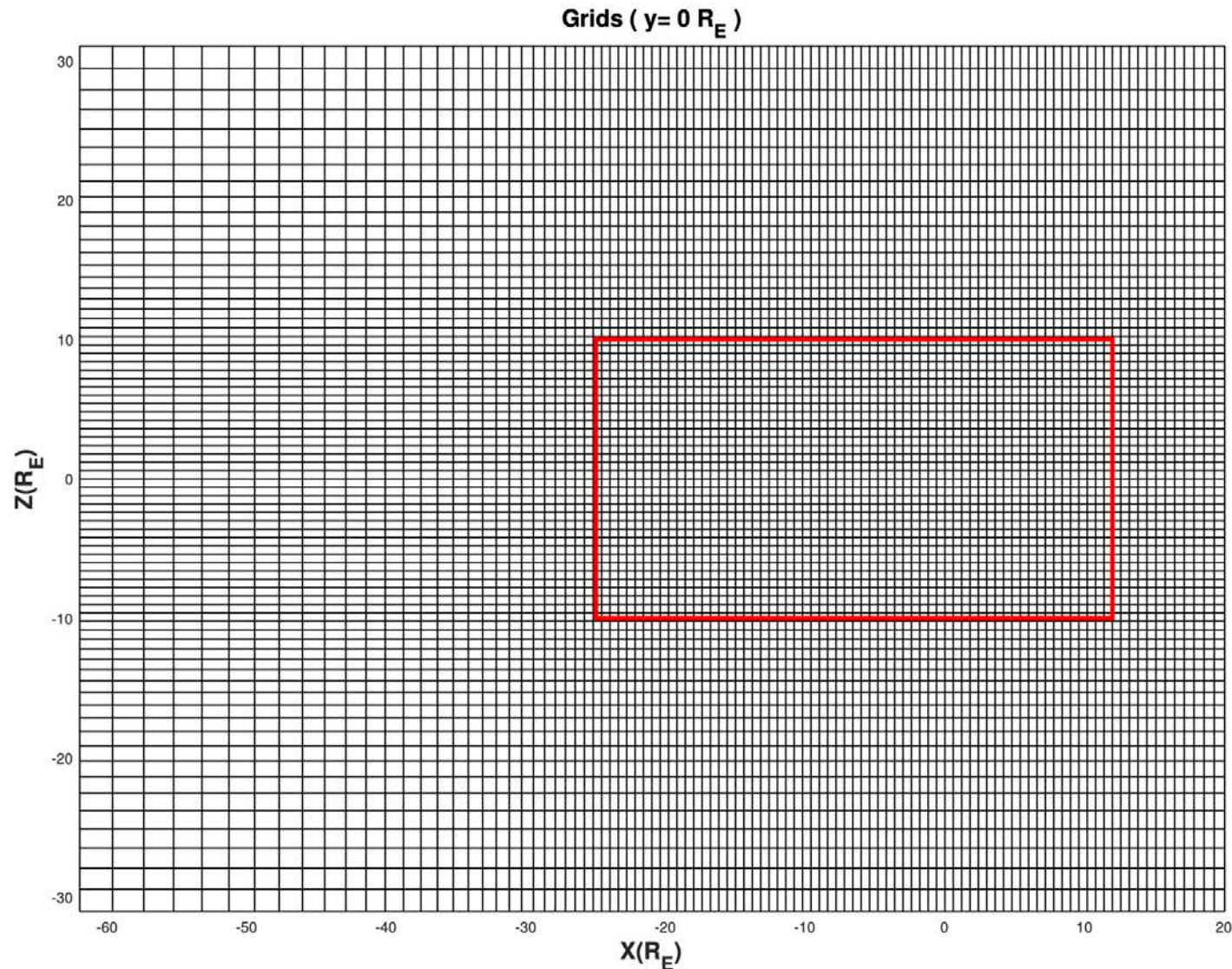
Fast magnetosonic/whistler



Ion Bernstein

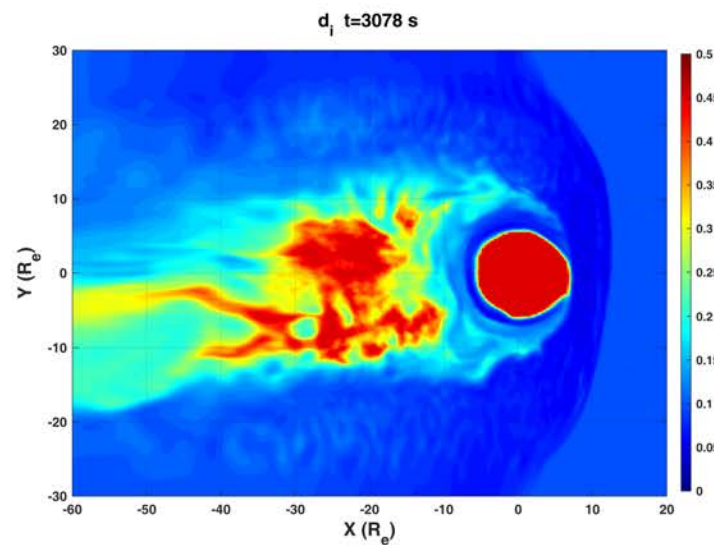
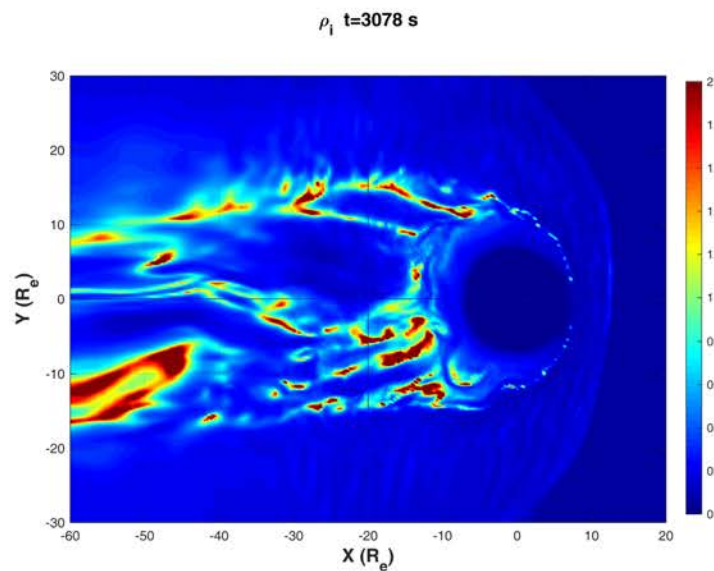
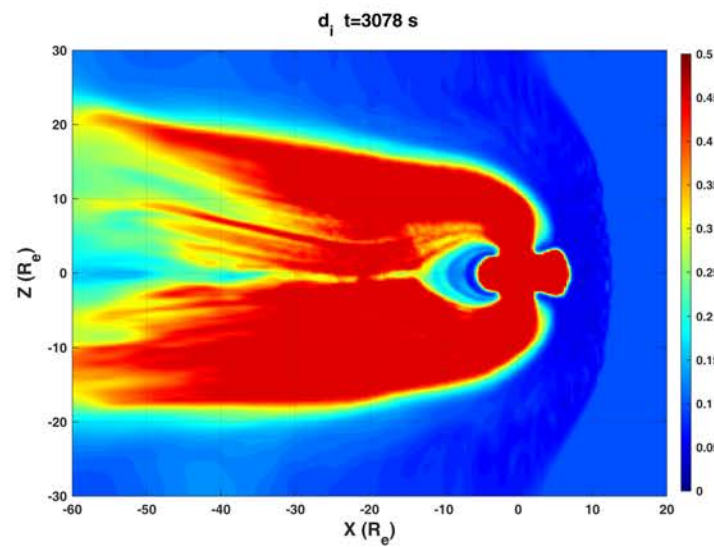
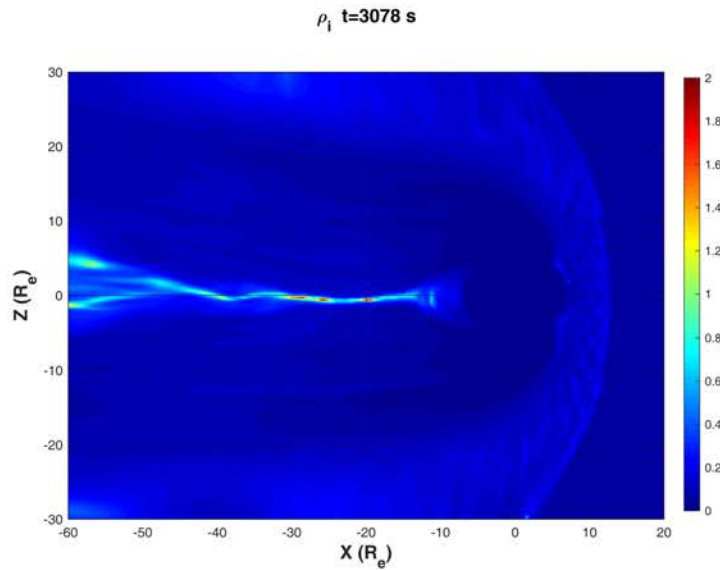


E.g., the benchmark against fully kinetic linear theory [Stix, 1992] in uniform plasma for $k_{\parallel}/k_{\perp}=0.1$ shows deviation between the two at $k\rho_i=3$.



Nonuniform cell grids, with a higher resolution ($0.15 R_E$) around the near-Earth plasma sheet ($x > -25 R_E$). Grid size < local ion initial length. Cell dimensions $N_x \times N_y \times N_z \approx 360 \times 250 \times 250$; totally $\sim 10^9 - 10^{10}$ particles.

Physical scale lengths to take into consideration



Parallel Computation – Load Balance

- Domain (field) and particle parallelization
- Balance of particle loading:

The simulation domain is divided into tens of thousands of small blocks, much more than the number of processors.

So that each processor handles tens to hundreds of blocks distributed randomly in the simulation domain.

So that the number of particles and the size of field array (thus memory) are loaded evenly over the processors.

Dynamic balance.

3. Results (1): generation of KAWs from the magnetotail to the ionosphere

Kinetic Alfvén waves observed in the magnetotail:

Magnetotail: Storm-time fast flow injections are associated with strong field-aligned currents that communicate the magnetic stresses to the ionosphere as shear Alfvén waves/KAWs in the PSBL [e.g., *Wygant et al.*, 2000; *Chaston et al.*, 2015].

Coupling between the fast flow energy & Alfvén waves: Auroral energy deposition during substorms [*Angelopoulos et al.*, 2002].

Inner magnetosphere: Kinetic field line resonance [*Chaston et al.*, 2014].

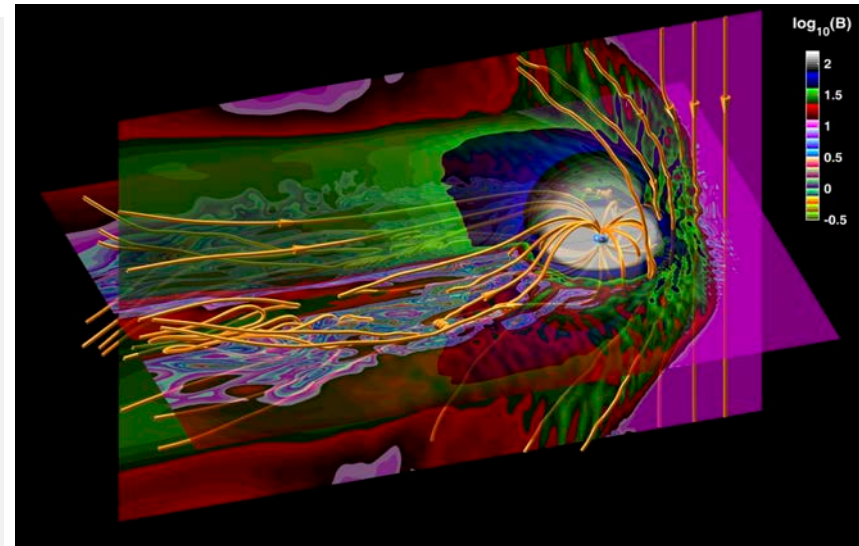
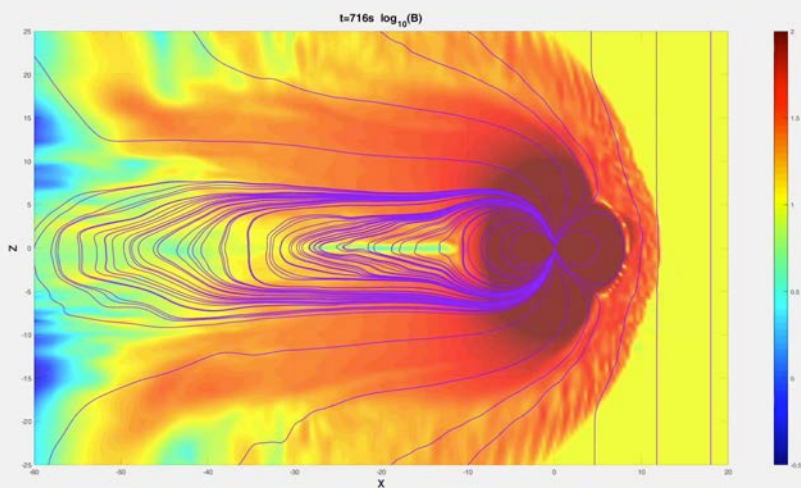
Connection among substorm onset and compressional waves at GOES, KAWs at FAST, and optical signatures at the ground [*Lessard et al.*, 2006, 2011]: Scenario of mode conversion from compressional wave to KAWs, propagating along field line.

KAWs associated with reconnection in the magnetotail [*Chaston et al.*, 2009; *Duan et al.*, 2016] and at the magnetopause [*Gershman et al.*, 2017].

3.1 ANGIE3D Global Simulation Results:

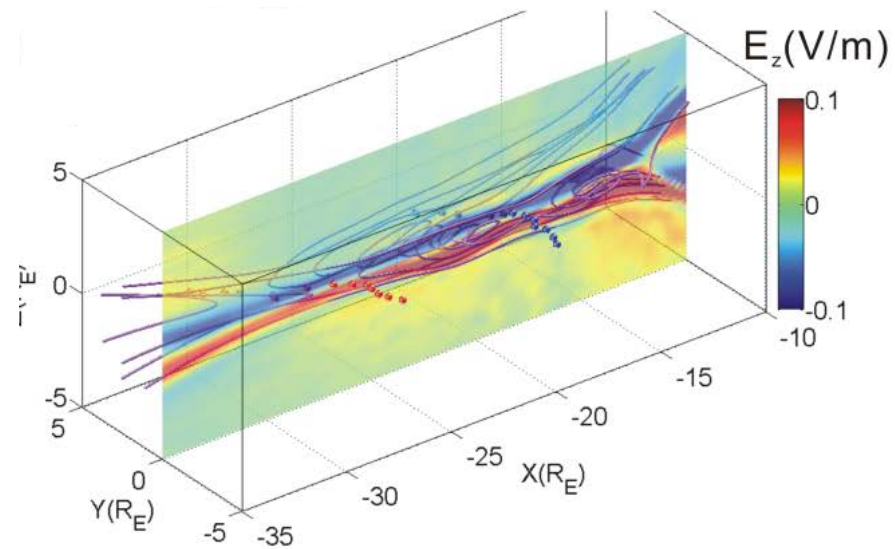
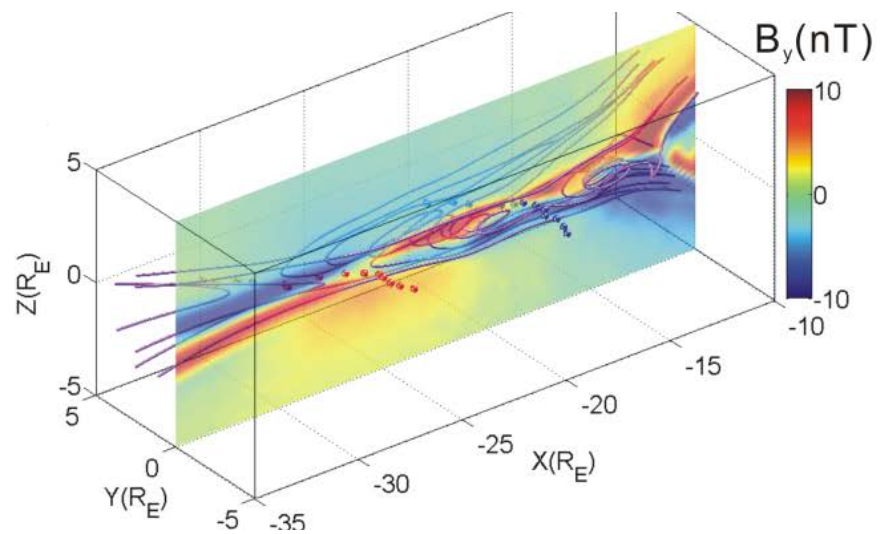
Case with a southward IMF, solar wind $M_A=7.8$, and $\beta_i=0.3$.

magnetic field

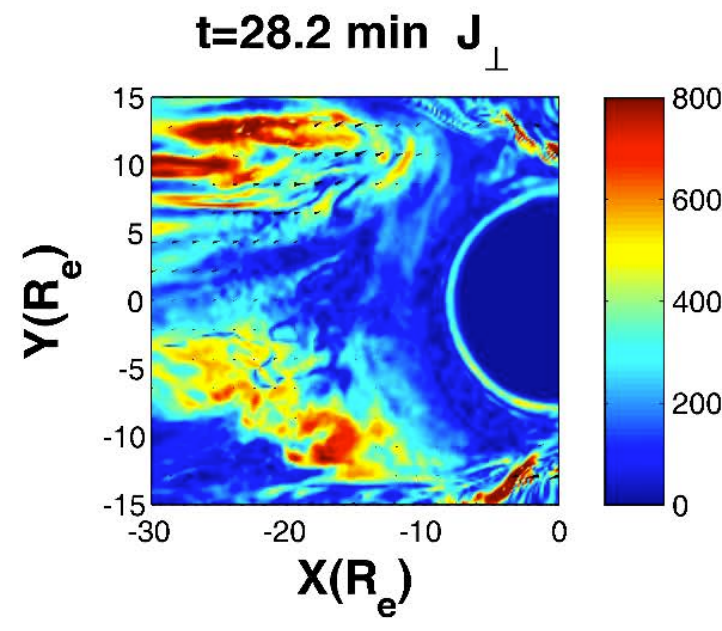
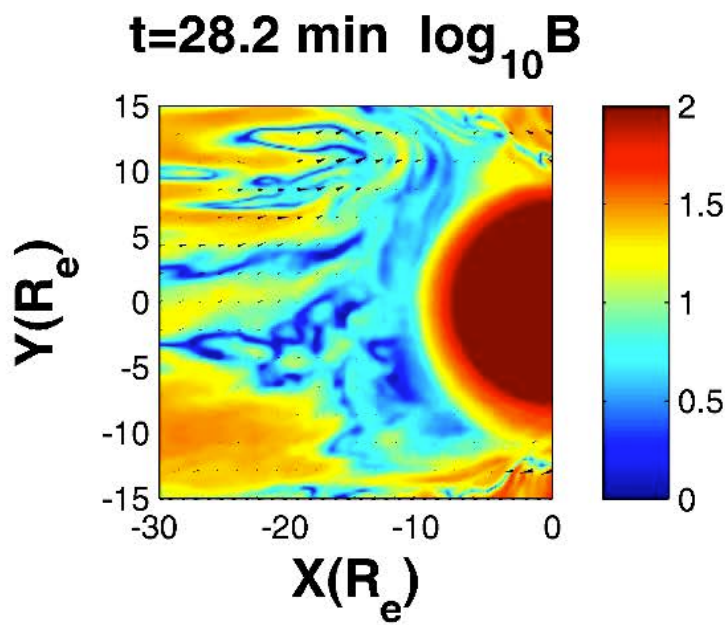
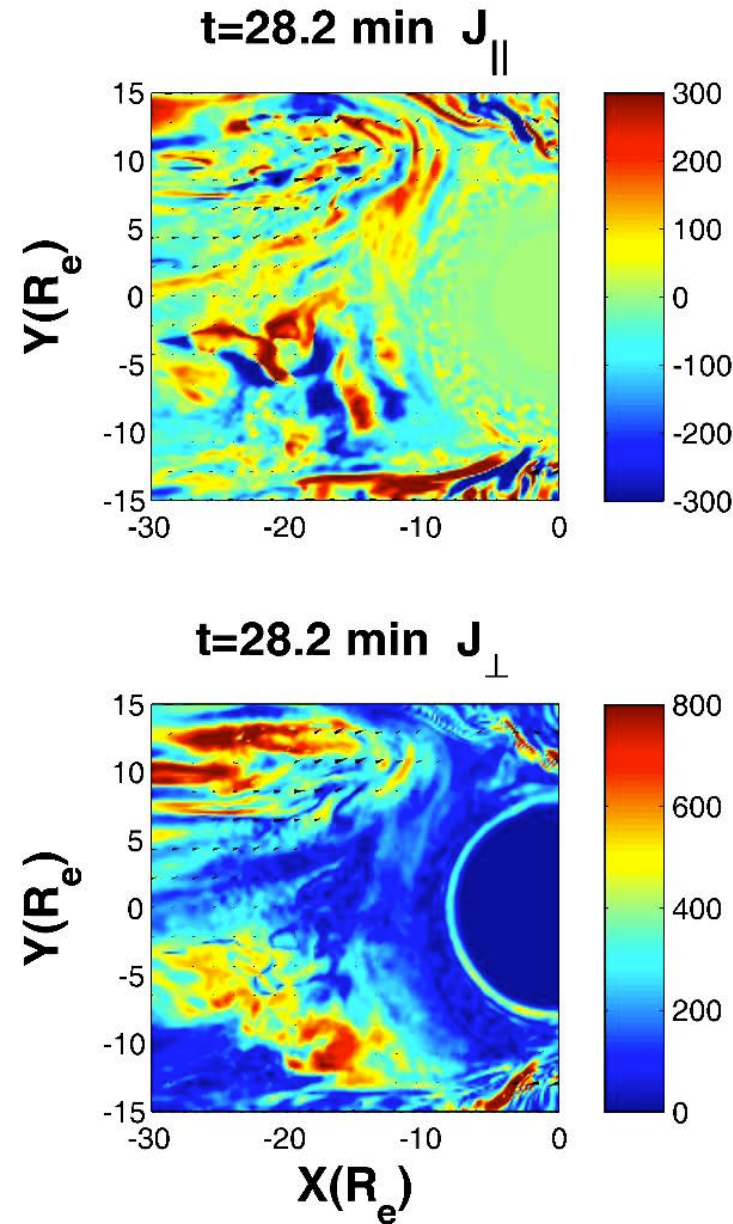
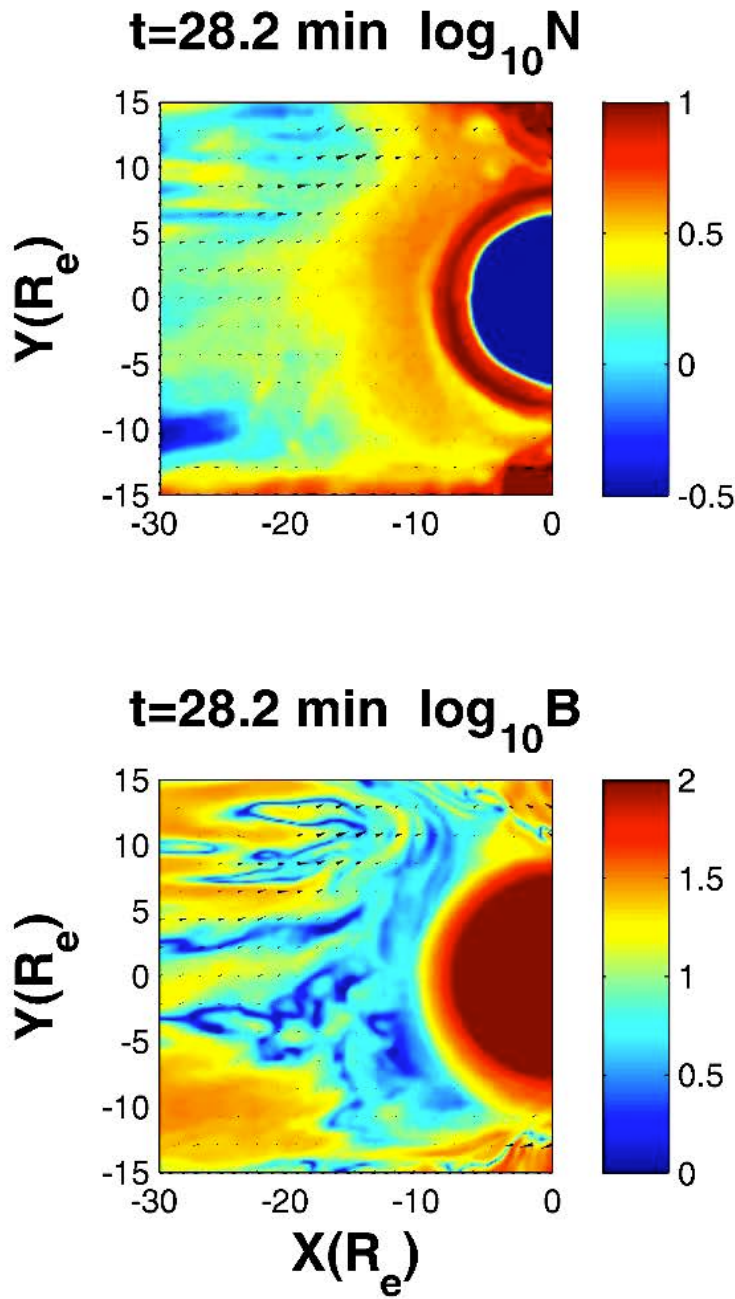


Magnetotail reconnection driven by a steady southward IMF

Tail reconnection: Hall quadrupolar B_y and E_z (midnight plane, $y=0$).

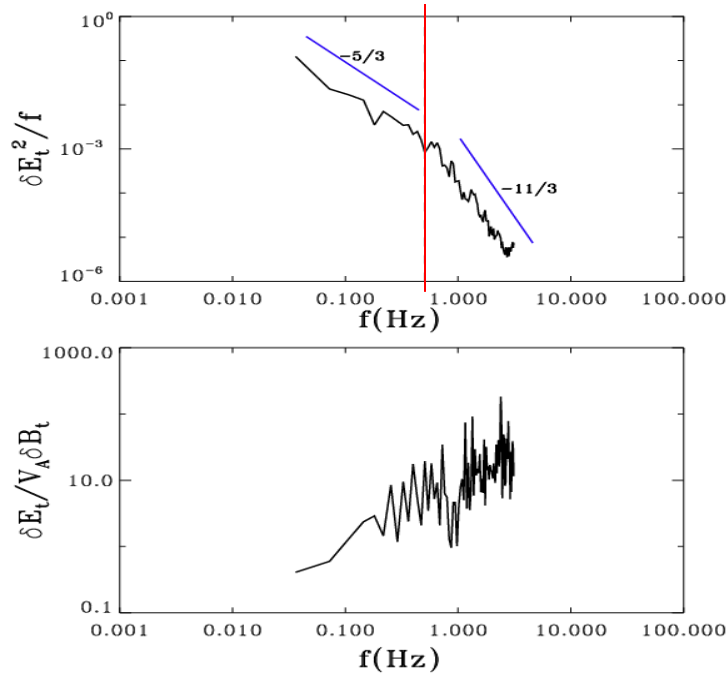


Equatorial structures associated with fast flows



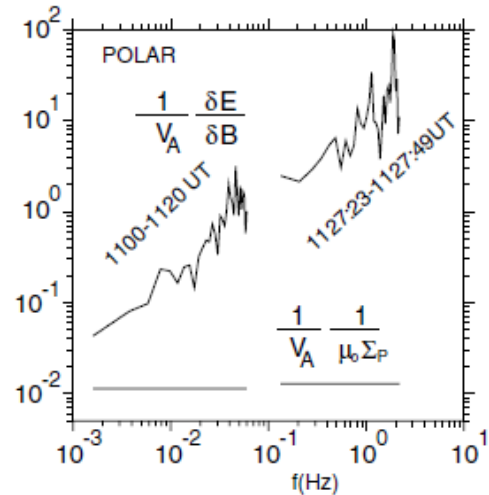
Shear Alfvén Turbulent Spectrum: Evidence of SAW and KAW waves?

ANGIE3D Simulation



Observation

[Angelopoulos *et al.*, 2002]

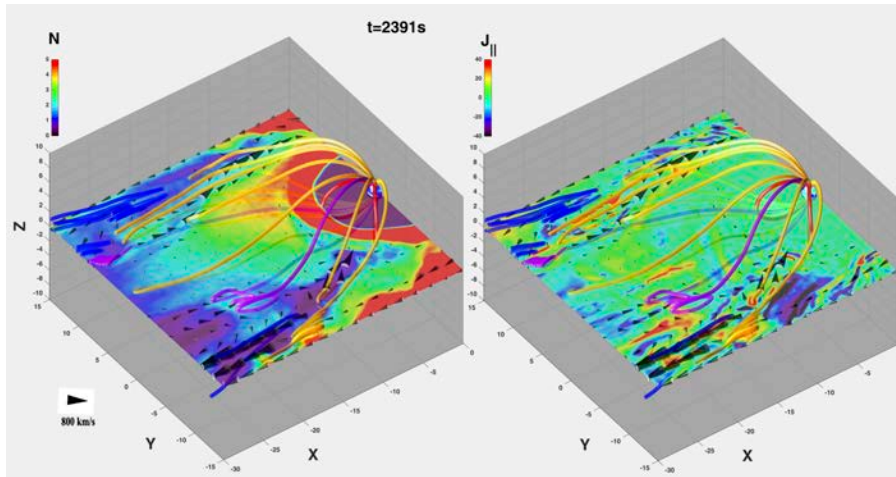


Spectra of (top) transverse electric energy density and (bottom) transverse E-to-B ratio in the PSBL obtained from the global hybrid simulation:

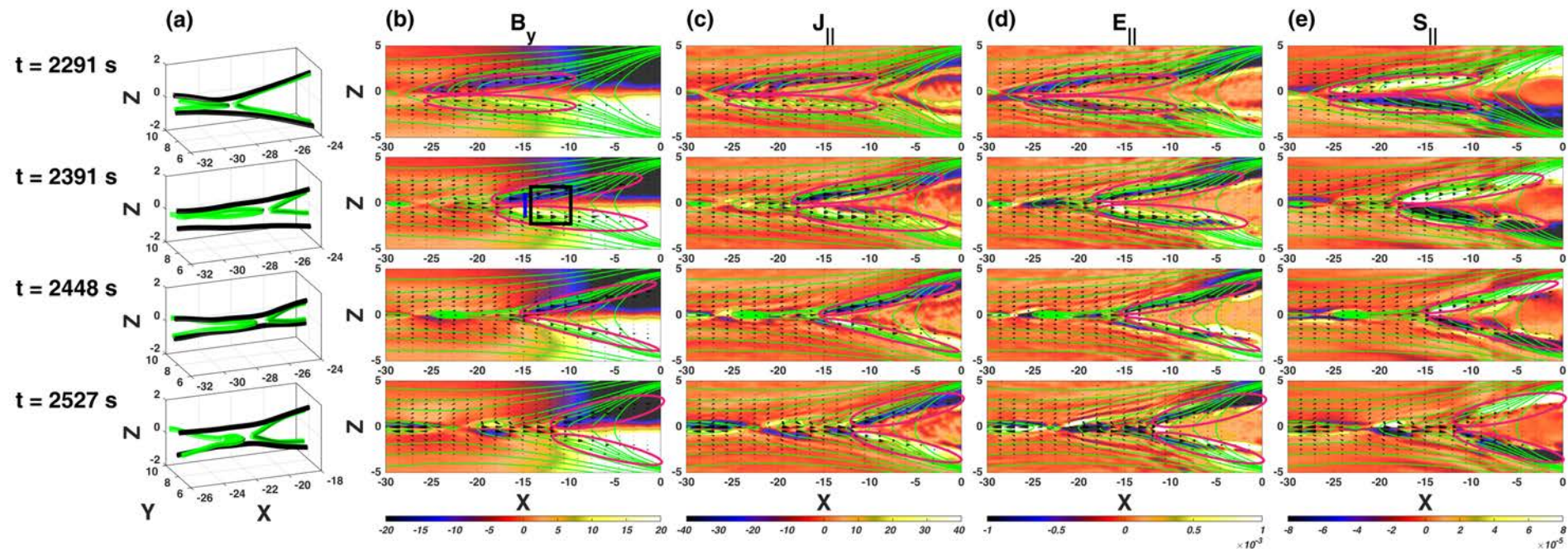
Spectral break at $\omega \sim \Omega_i$ ($k\rho_i \sim 1$), the energy sink at cross-scale coupling in the turbulence spectrum.

The polarization ratio is consistent with the KAW dispersion relation.

Equatorial plane, $z = 0$:

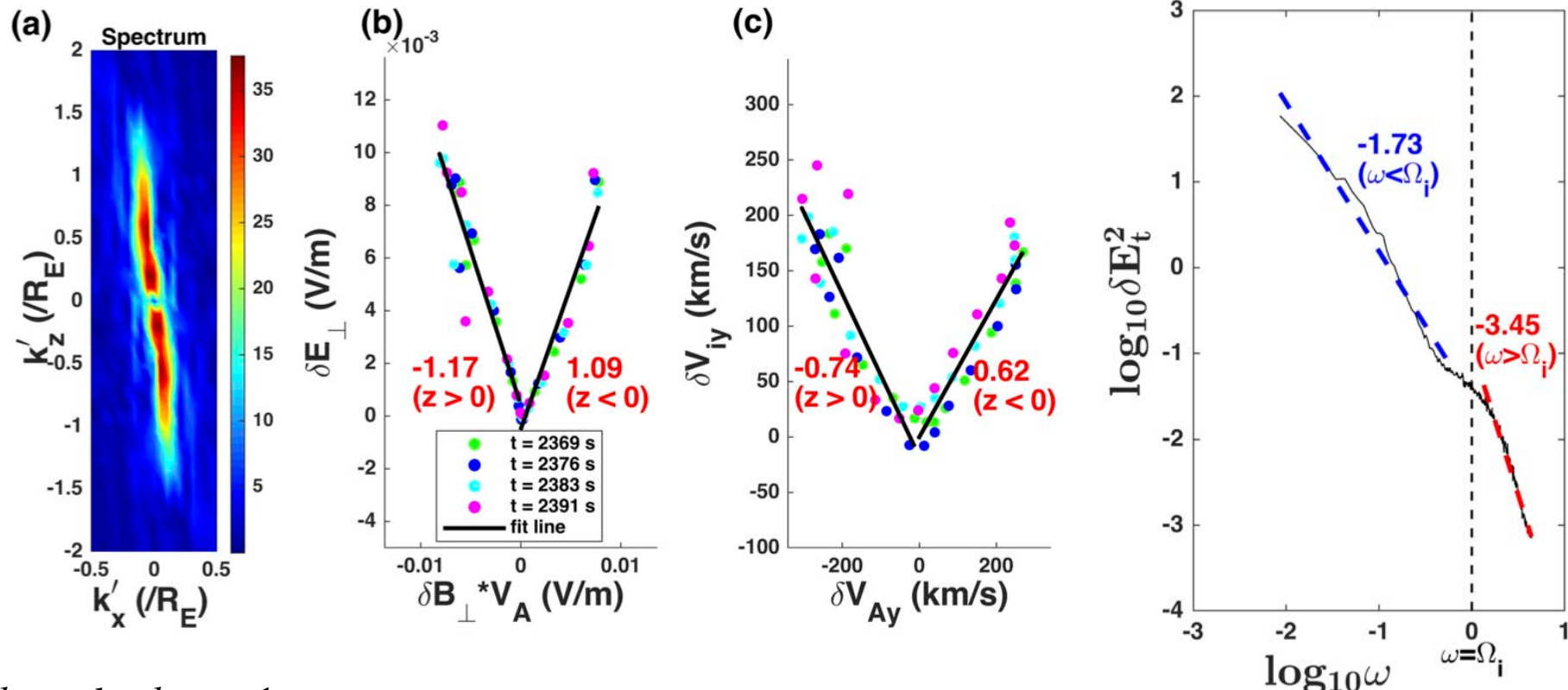


Plane of $y = 8 R_E$:



[Cheng et al., JGR, 2020]

Identification of Kinetic Alfvén Waves (KAWs)



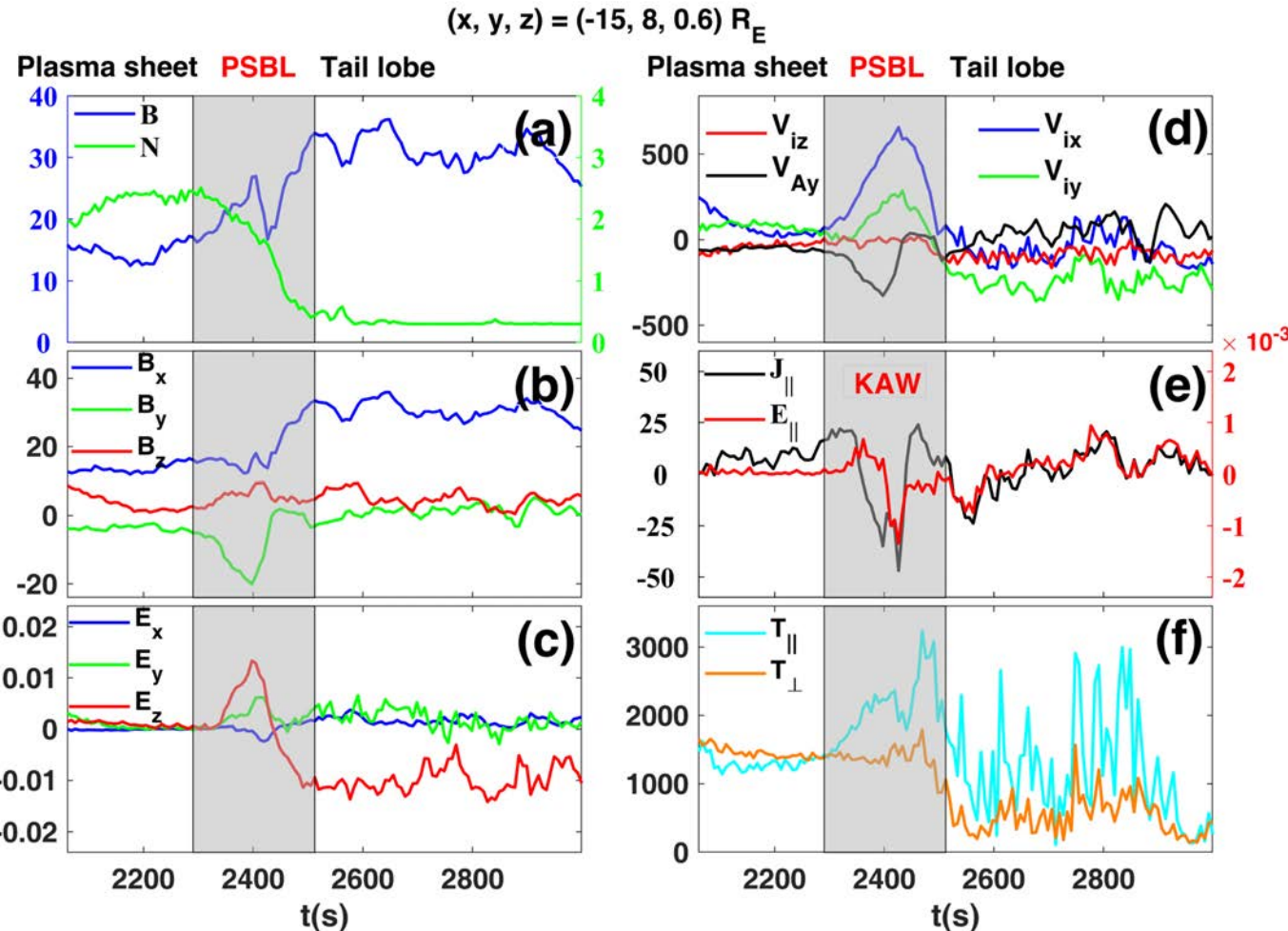
$k_{\perp} \gg k_{\parallel}$. $k_{\perp} \rho_i \sim 1$,
super-Alfvénic speed;

$$\omega^2 = k_{\parallel}^2 V_A^2 [1 + (1 + T_e/T_i) k_{\perp}^2 \rho_i^2]$$

Polarization Relation

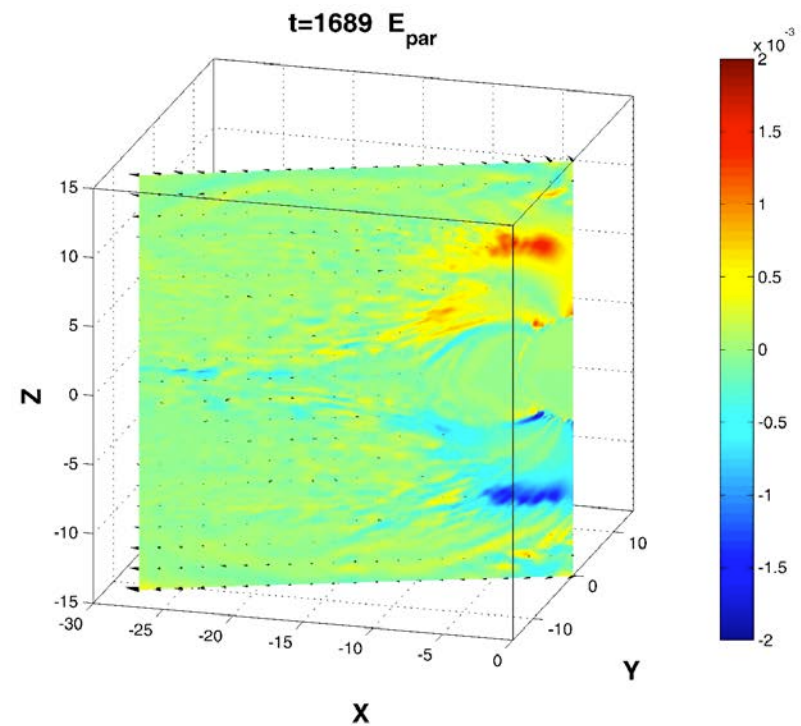
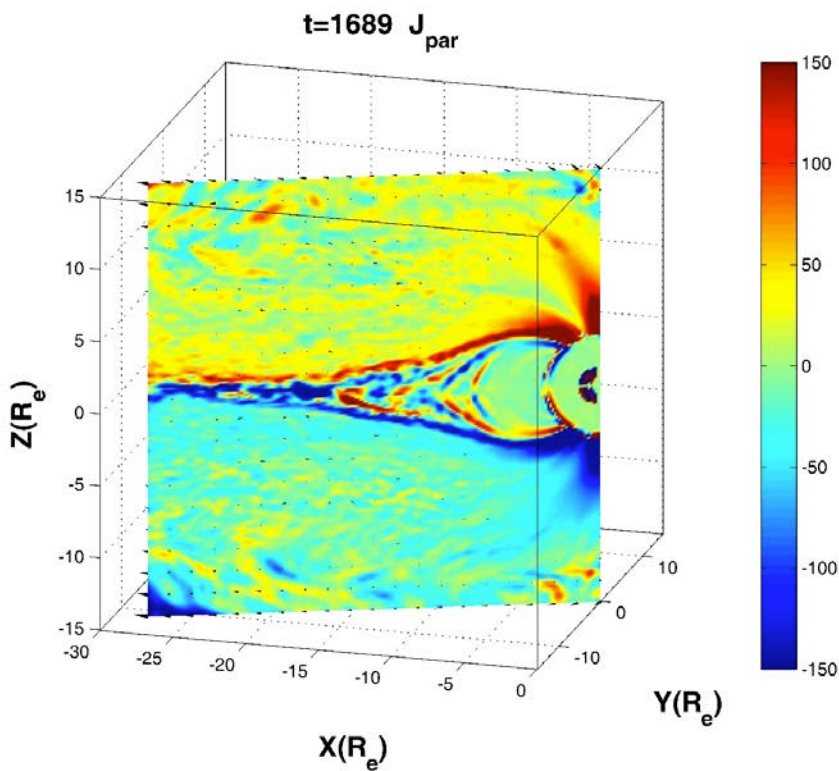
Power spectrum

KAW signature in a virtual spacecraft crossing:
Time variations at a fixed location in the plasma sheet boundary layer (PSBL)



- Background magnetic field is dominated by B_x (northern hemisphere).
- Perturbations of B_y , E_z , and J_{\parallel} are well correlated.
- Anti-phase relation between V_{iy} and V_{Ay} : KAW propagates along \mathbf{B} to the ionosphere.
- Parallel electric field E_{\parallel} is excited.

Propagation of SAWs/Field-Aligned Currents



Possible Mechanisms for the Generation of KAWs

- **Reconnection** in the plasma sheet:

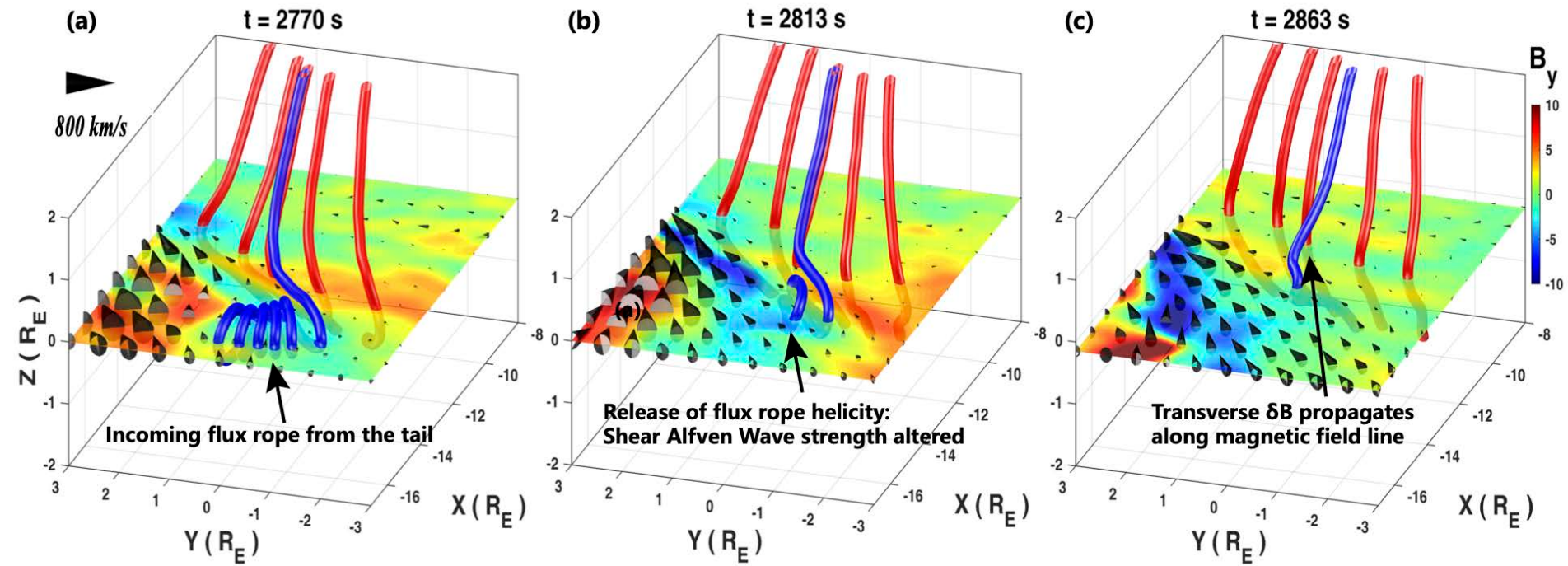
Hybrid simulation of local current sheet [*Liang et al.*, JGR, 2016; PoP, 2017]: δB_y due to ion Hall effects propagates as 3D KAWs carrying **E** and **B** polarizations and parallel Poyning flux.

- **Fast flow braking** region in front of the dipolar field.
- Mode conversion from the abundant compressional waves (generated in the plasma sheet & the flow braking) in the nonuniform plasma in front of the dipole-like field.

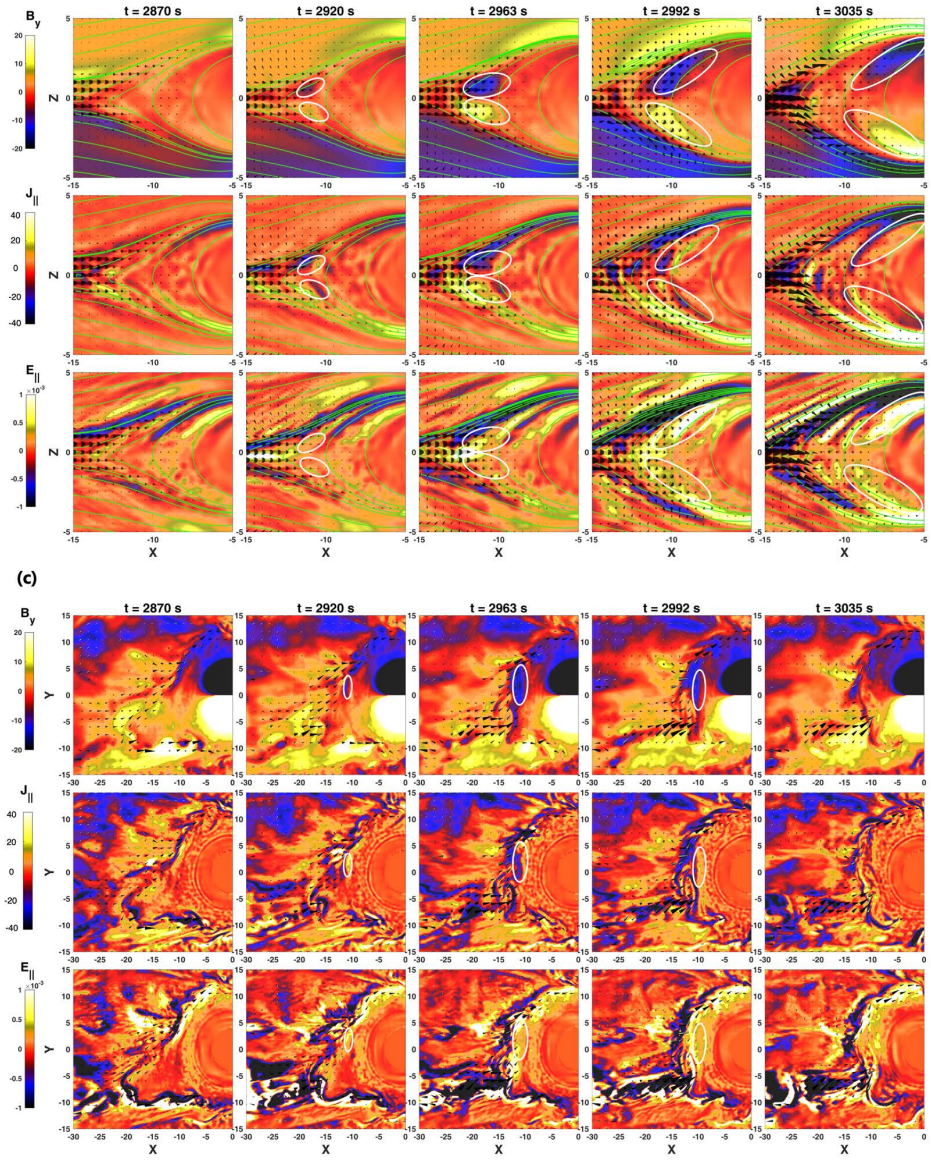
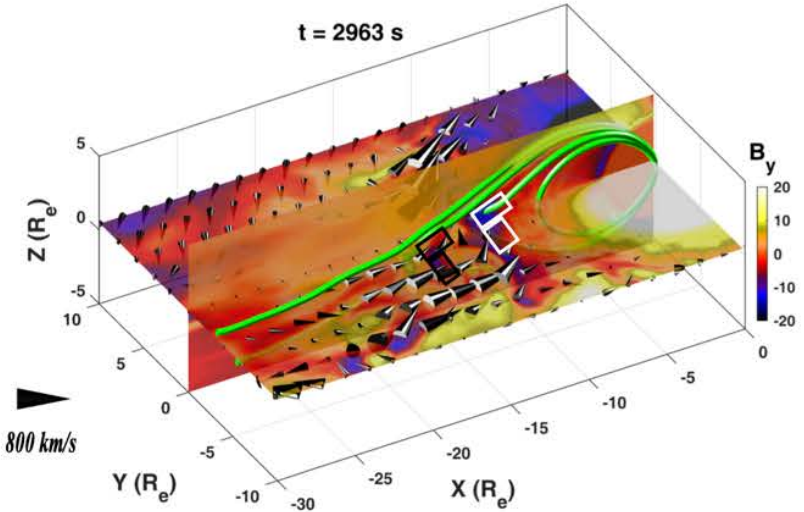
Phase mixing of shear Alfvén waves in nonuniform plasma.

- Alfvénic ion beams from the tail: Interaction with the dipole-like field.
- Turbulent cascade to short wavelengths.

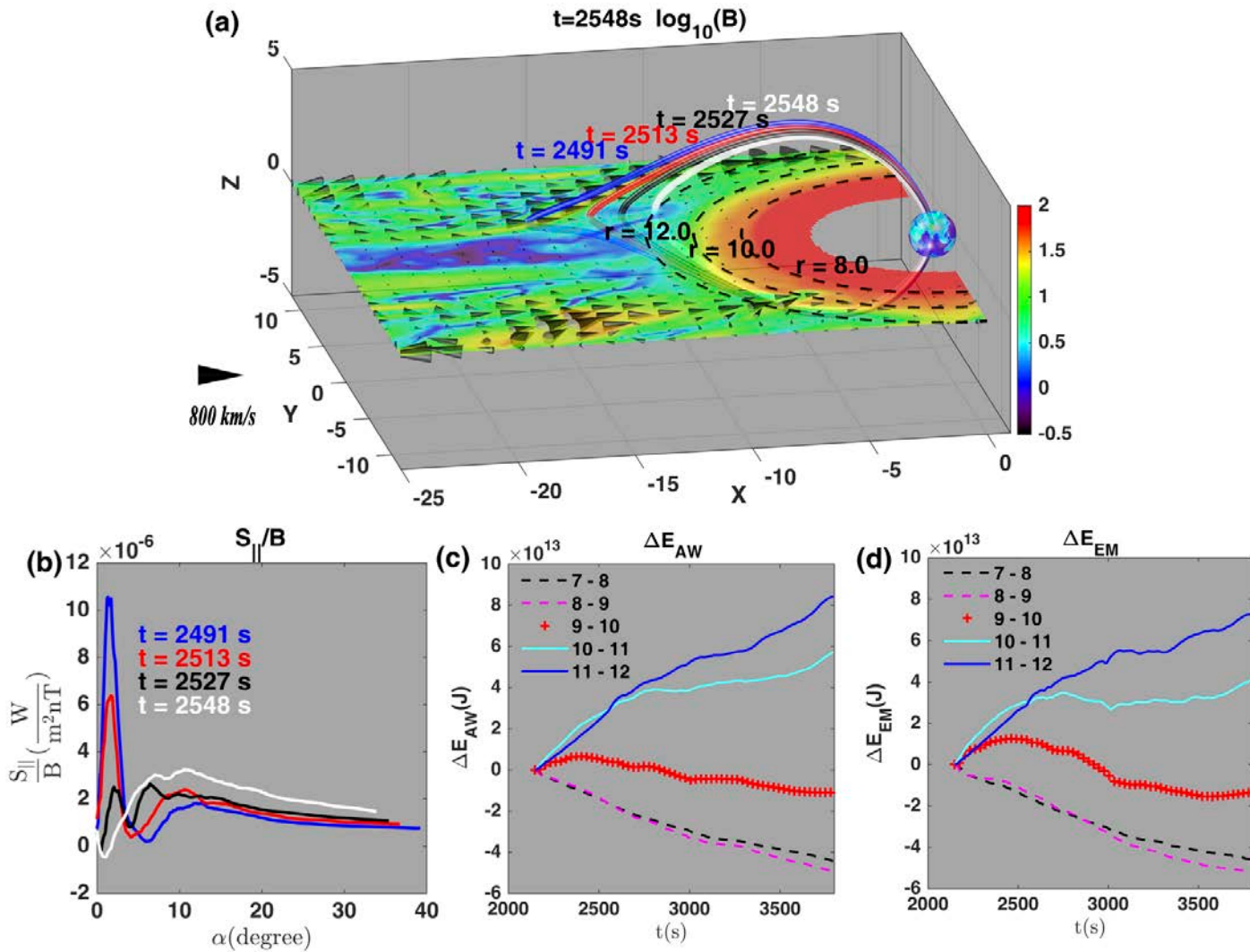
Flow Braking Region: Interaction between *Flux Ropes* and the *Dipole-Like Field*



KAWs in the dipolar magnetic field region



Transport of KAWs and energy conversion



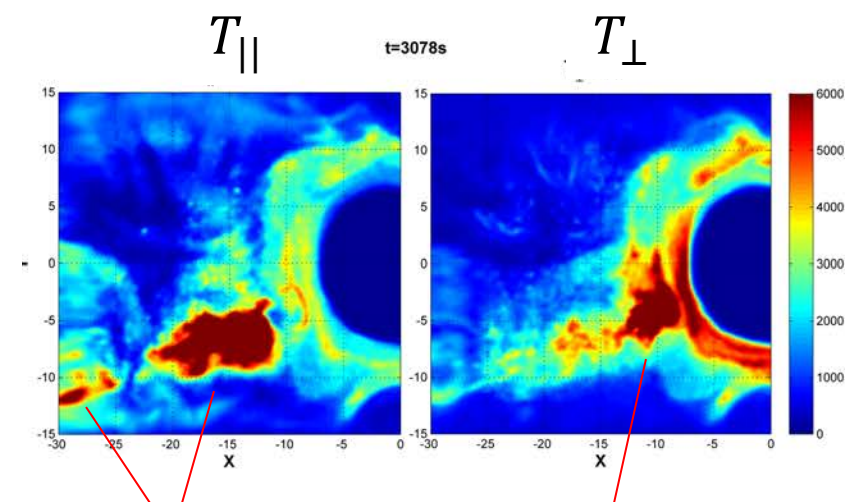
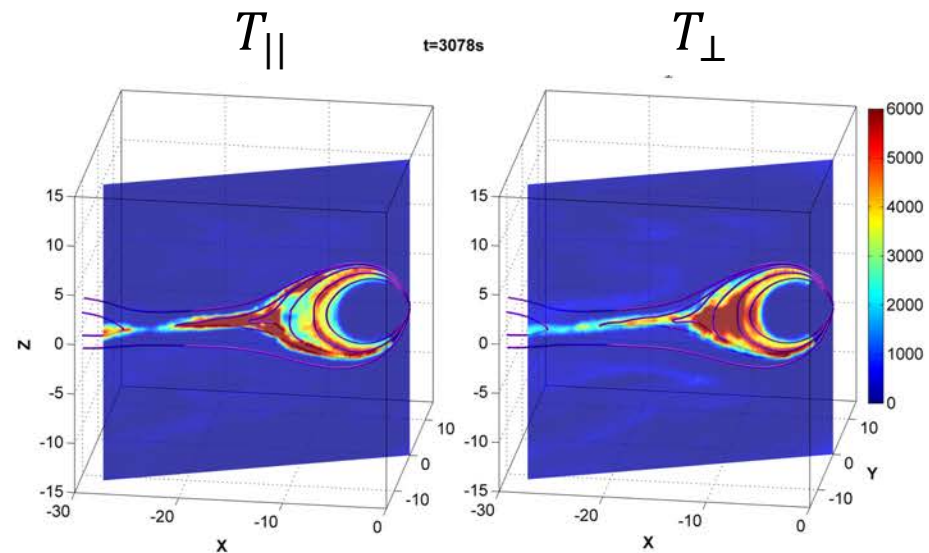
(a) Equatorial contours of B and convection of a field line.

(b) S_{\parallel}/B vs. latitude α along the field line at various times.

Time evolution of (c) Alfvénic wave energy (ΔE_{AW}) and (d) electromagnetic wave energy (ΔE_{EM}) flowing out of the nightside spherical shells as a function of time.

Effects of Waves/Turbulence on Ion Transport to the Inner Magnetosphere

Ion Heating associated with the Wave Activities



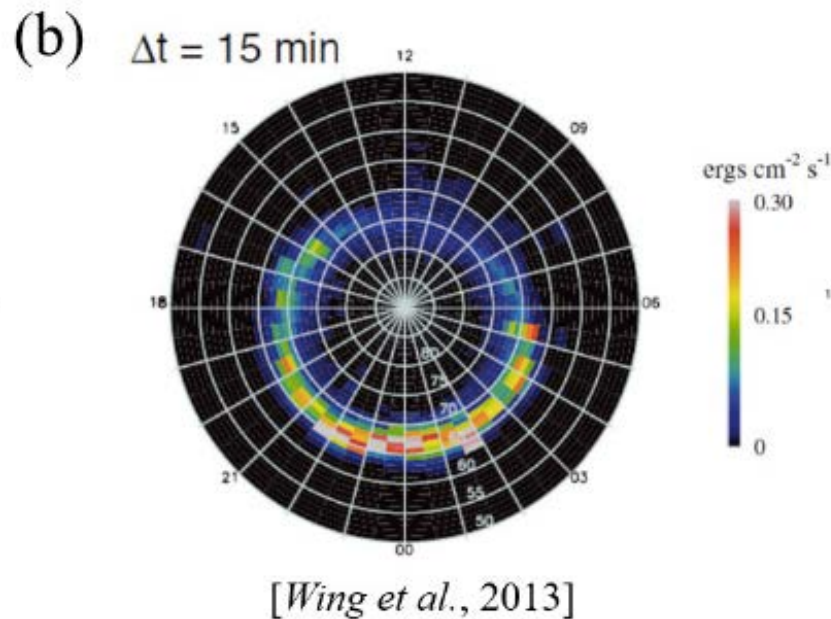
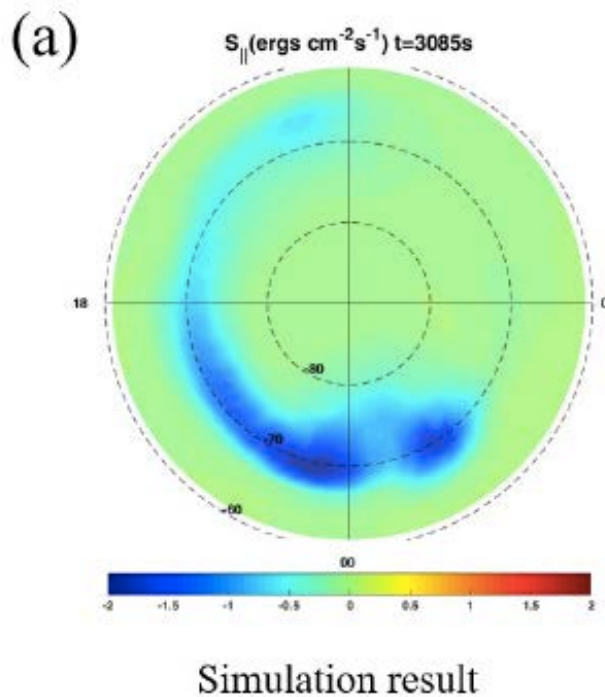
$T_{||} > T_{\perp}$ in reconnection

Heating in T_{\perp} at
the flow braking

Temperature in the meridian plane
of a fast flow event

Temperature in the equator

- Comparison with the DMSP (ionosphere) observation:



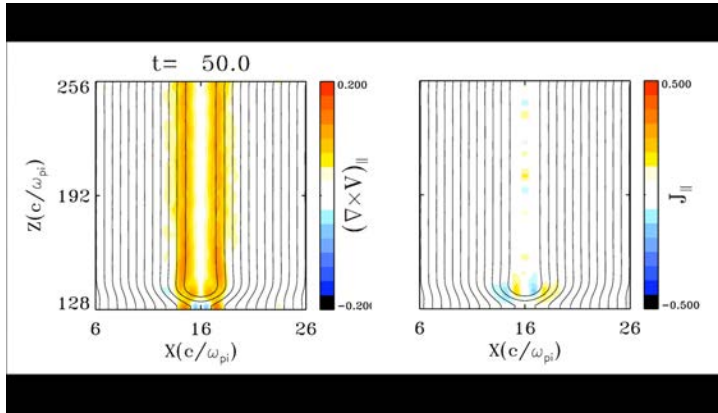
Statistical result of DMSP
satellites from 1996 to 2007:
Aurora ion energy flux 15 min
after the substorm onset.

3.2 Comparison with local hybrid simulations

Generation of KAWs by magnetic reconnection and the associated ion heating

Hybrid simulation in slab geometry: Generation of KAWs in reconnection [Liang et al., 2016]

Case with localized v_c X-line length $\xi=\infty$ (2-D like) ,and $B_{y0}=0$

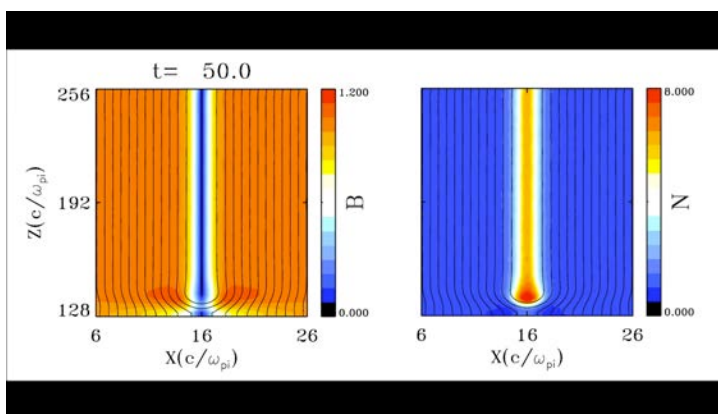


Structure in the xz plane:

- KAWs are present throughout the reconnection bulge.
- (1) Parallel vorticity \approx parallel current density;
- (2) Magnetic field and density perturbations are anti-phase.
- (3) Wave front propagation: away from the diffusion region with $V_{ph}=1.1V_{A0}$

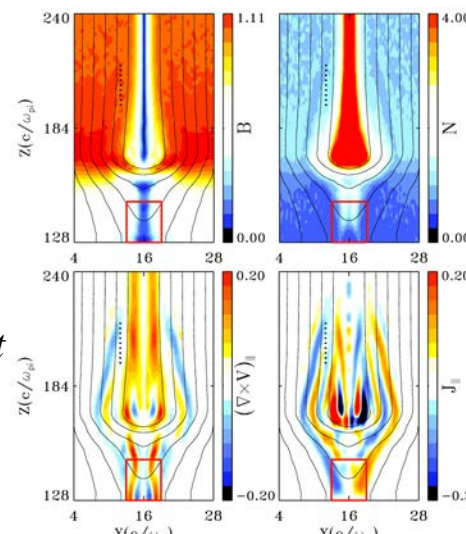
$$\omega^2 = k_{\parallel}^2 V_A^2 [1 + (1 + T_e/T_i) k_{\perp}^2 \rho_i^2]$$

KAWs: $k_{\perp} \rho_i \sim 1$, super-Alfvenic speed; $k_{\perp} \gg k_{\parallel}$.



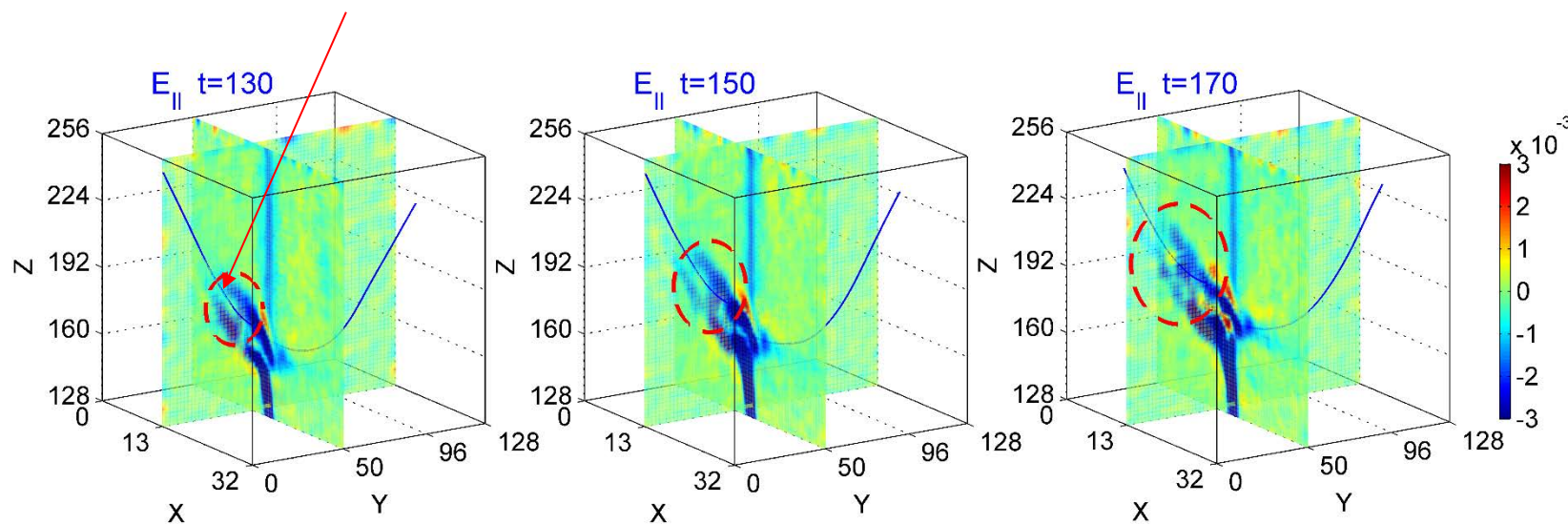
B vs. N

parallel vorticity vs. parallel current



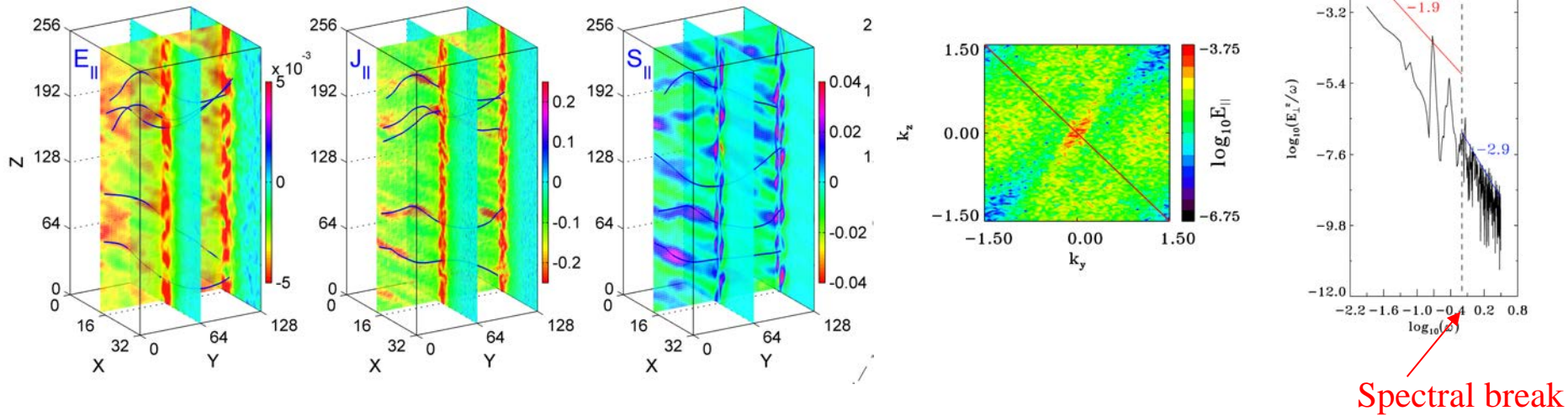
Case: localized v_c , X-line length = $10d_{i0}$ and $B_{y0}=0.5B_{z0}$

3-D KAW pulses propagating along the oblique magnetic field lines



Estimated damping rate (ion physics only): $\sim -0.005 \Omega_{i0}$, or decay time $\sim 160-280 \Omega_{i0}^{-1}$, ~ 10 wave periods.
 $S_{\parallel} \sim 0.1 \text{ erg cm}^{-2}\text{s}^{-1}$ under the magnetotail conditions.

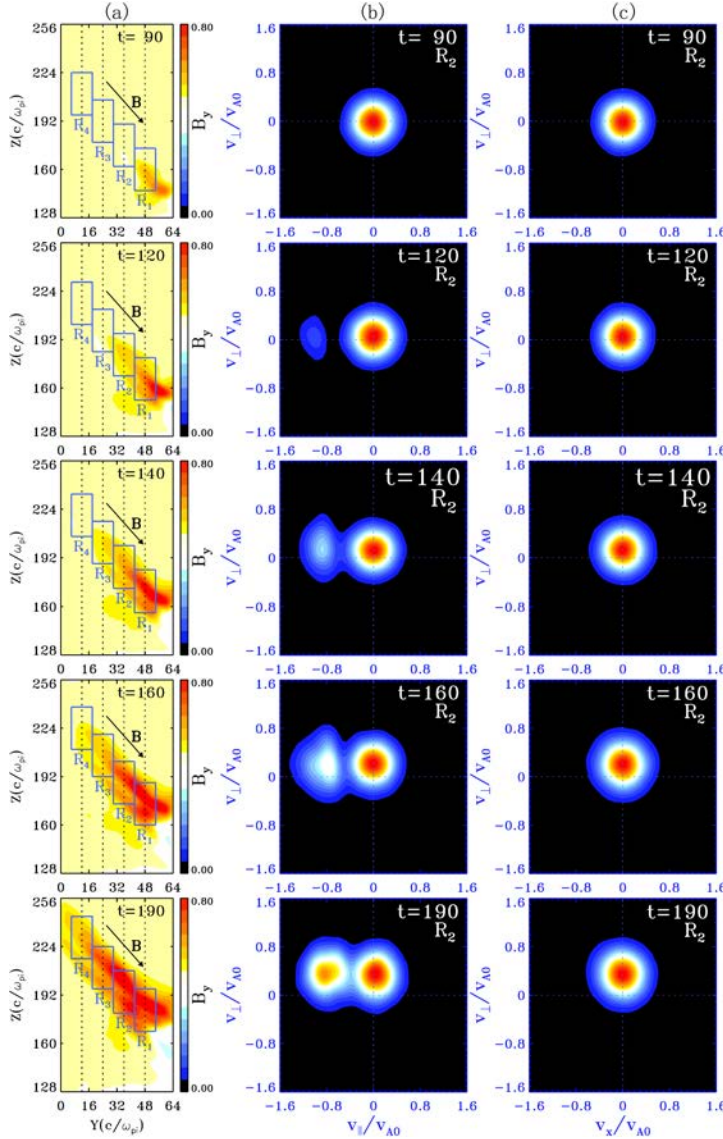
Case: current-dependent resistivity, guide field $B_{y0}=0.5B_{x0}$



Ion Acceleration and Heating by KAWs in 3D Reconnection [Liang et al., 2017]

Time evolution of ion distribution along the path of KAWs

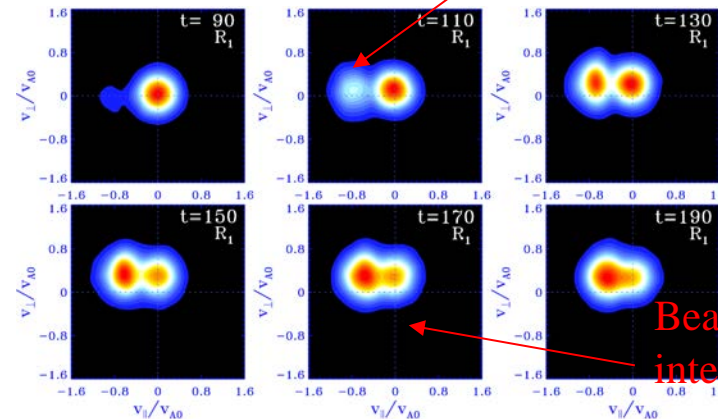
at location R_2 :



at location R_1 :

(farther, with later time interaction)

Accelerated ion beam



Beam-plasma
interaction

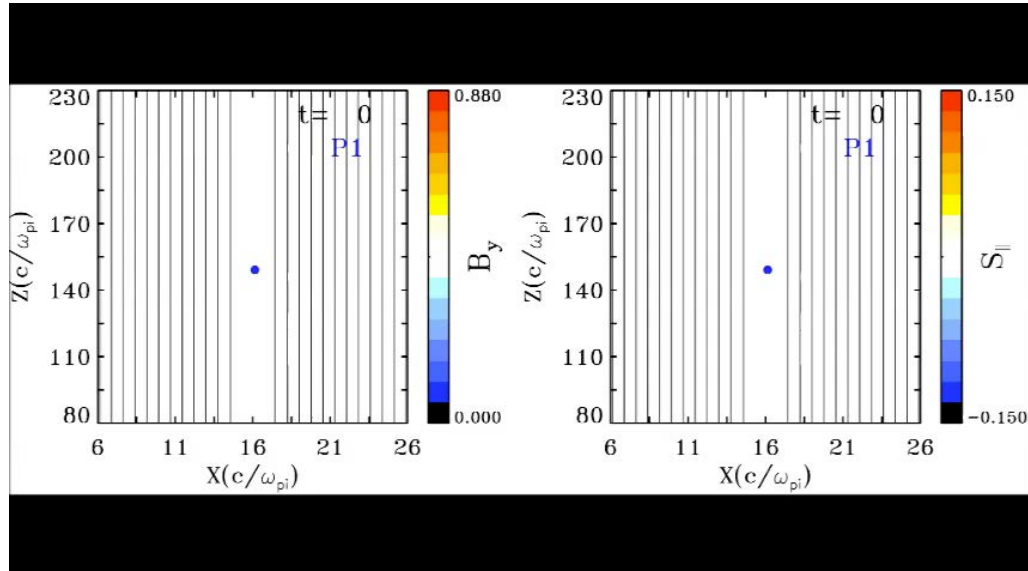
Main results:

- $t < 160$: (1) Acceleration of ions by KAWs → trapping by wave potential;
- (2) T_{\parallel} heating of the accelerated beam by Landau resonance;
- (3) Simultaneous stochastic $T_{\perp} (> T_{\parallel})$ heating of the beam.

$t > 160$: Interaction between the accelerated beam and the core plasma → heating.

Overall, $T_{\parallel} > T_{\perp}$.

Particle trajectory: Ion trapping in the KAWs, parallel acceleration



Estimate of nonlinear bounce frequency of trapped ions

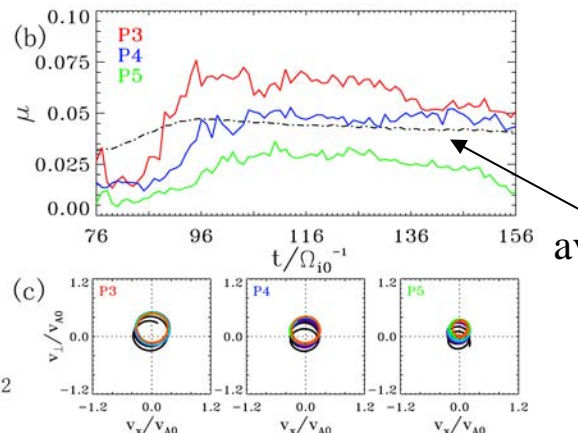
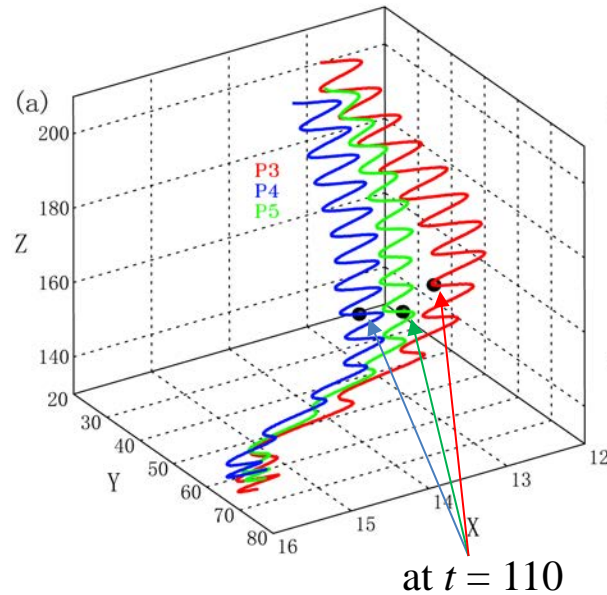
- Due to $E_{||}$: $m_i\omega_B^2x \sim (e\delta E_{||})(k_{||}x)$
 $\Rightarrow \omega_B/\Omega_i \sim (\delta E_{||}/\delta E_{\perp})^{1/2} (ek_{||}\delta E_{\perp}/m_i)^{1/2}/\Omega_i$.

Faraday's law: $k_{||}\delta E_{\perp} \sim \omega \delta B_{\perp}$
 $\omega_B/\Omega_i \sim (\delta E_{||}/\delta E_{\perp})^{1/2} (\delta B_{\perp}/B)^{1/2}(\omega/\Omega_i)^{1/2}$

From simulation data, $\omega_B/\Omega_i \sim [(0.0015/0.1)(0.15)(1/5)]^{1/2} \sim 1/50-1/30$.
 Bounce period $\sim 30-50\Omega_i^{-1}$

- Due to magnetic mirror force:
 $F = |\mu \nabla_{||} B| \sim (m_i v_{\perp}^2 / 2B_0) k_{||} \delta B_{||}$.
 Bounce period $\sim (\rho_i^2 k_{||}^2 \Omega_i^2 \delta B_{||}/B)^{-1/2}$
 $\sim 35\Omega_i^{-1}$
- Measured particle guiding center parallel bounce frequency:
 $\sim 30-60\Omega_i^{-1}$

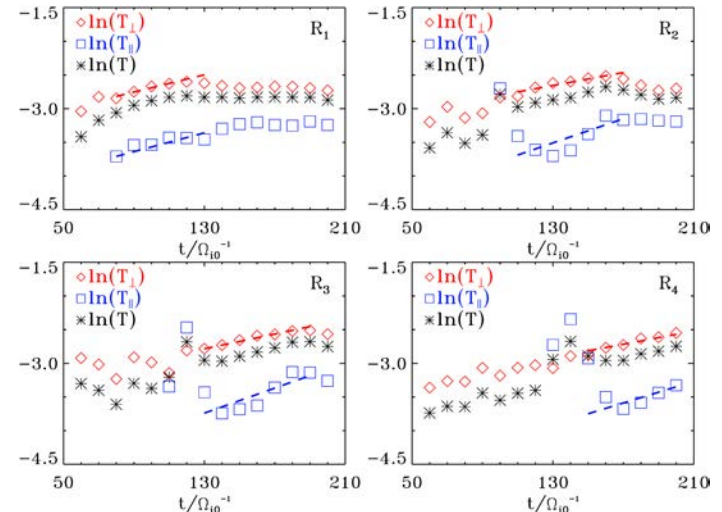
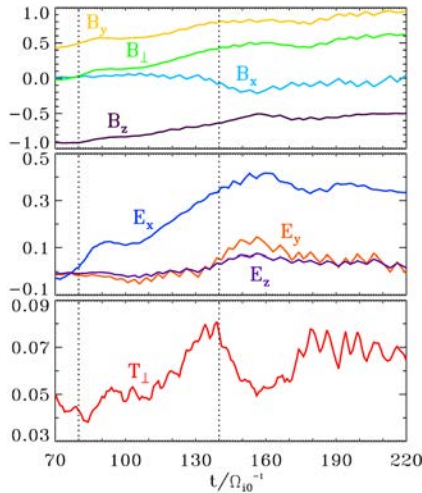
Perpendicular Stochastic Heating



Trajectories of three particles and time evolutions of their μ and velocities.

average of about 800 particles

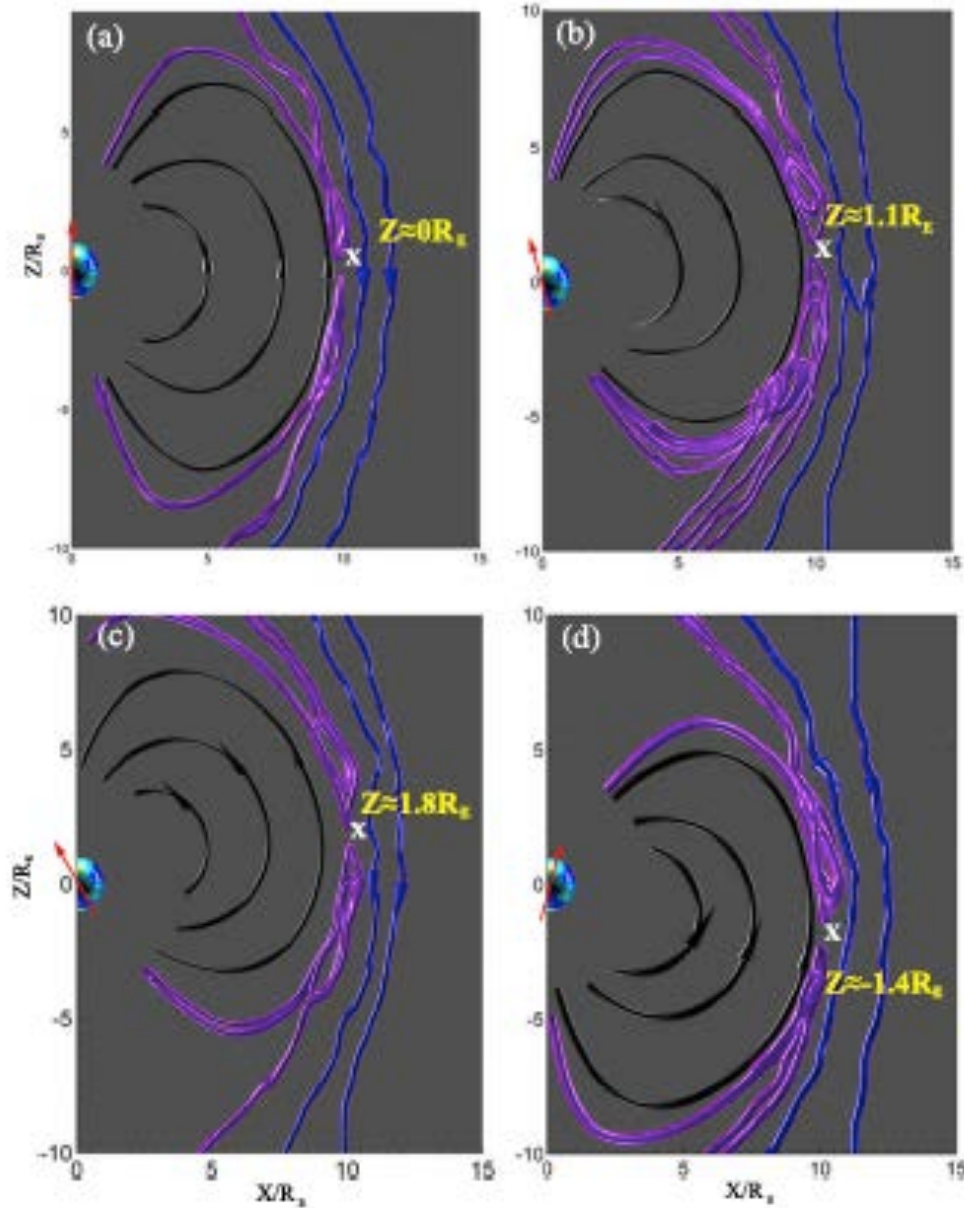
Time evolutions in region R1 in KAWs.



Heating rate $\gamma_\perp/\Omega_{i0} \sim 0.0047\text{--}0.0066$, parallel $\gamma_\parallel/\Omega_{i0} \sim 0.0068\text{--}0.0093$. Consistent with the estimated damping rate $\sim 0.0035\text{ -- }0.0062$ of KAWs. Electron acceleration: electron test particle simulations in hybrid run.

4. Results (2): magnetopause reconnection and comparison with MMS observations

Guo et al. [2020]



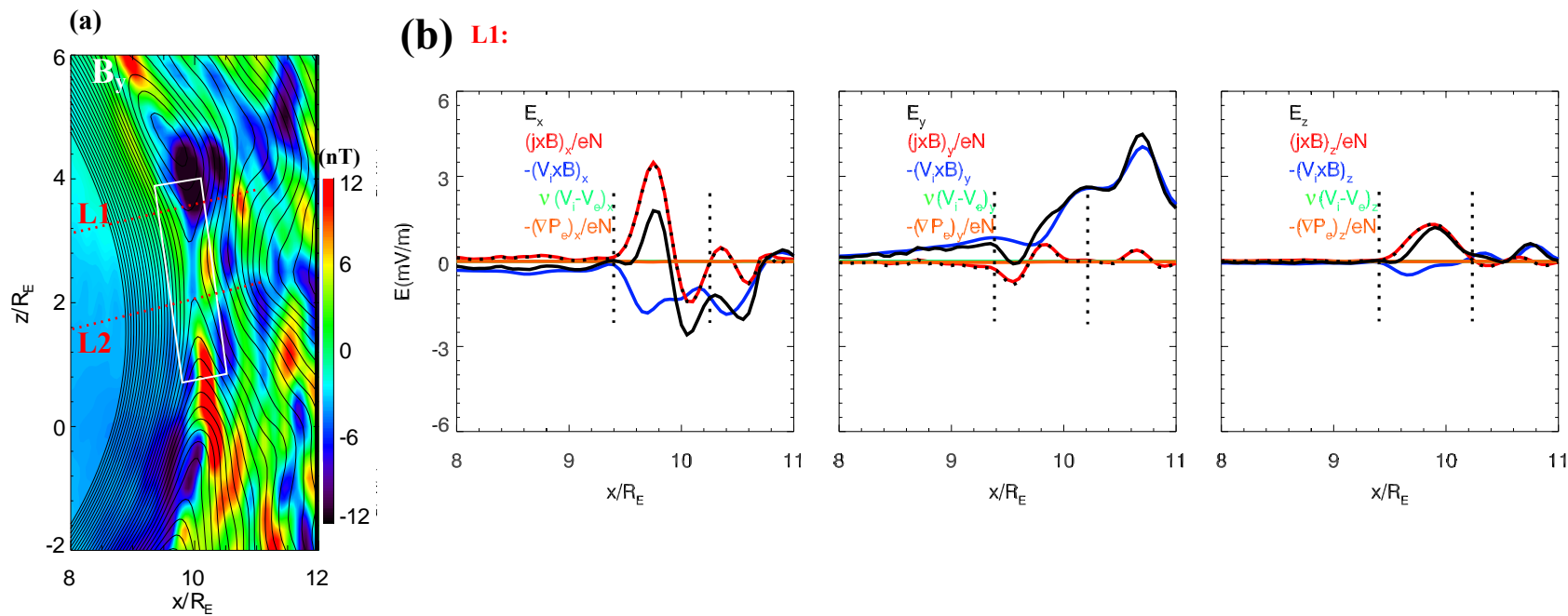
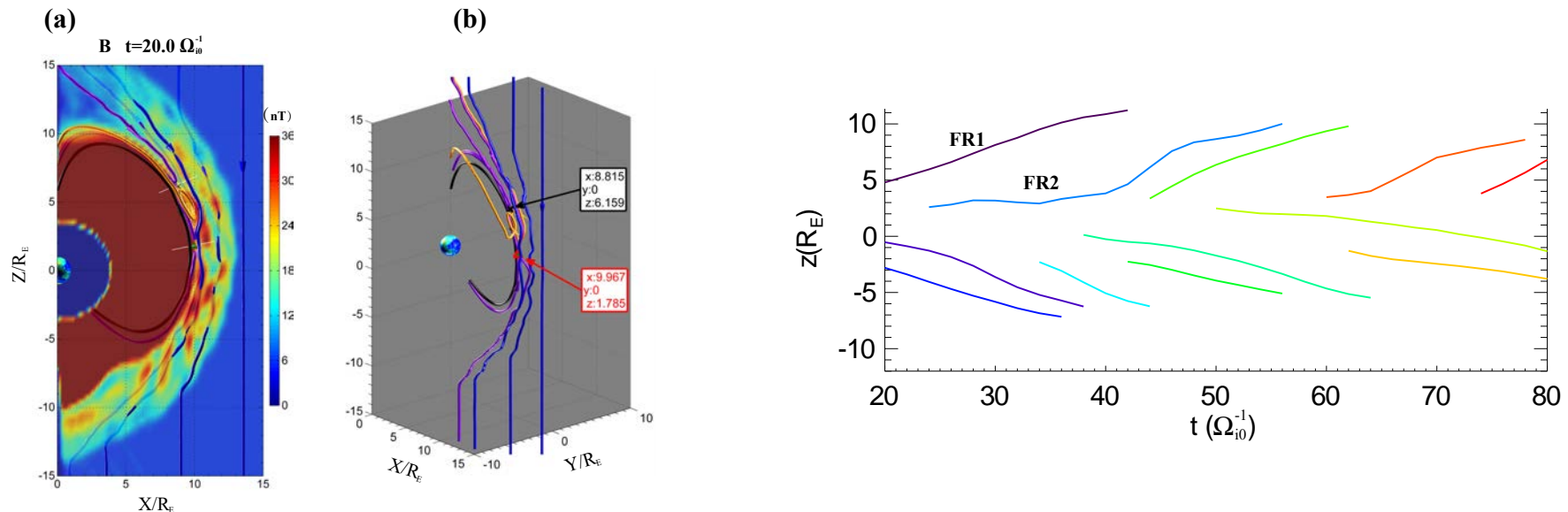
Field line configuration in the noon meridian plane:

- Cases with the dipole tilt angle of
- (a) 0° ($Z_X \sim 0$)
 - (b) -15° ($Z_X \sim 1.1 R_E$)
 - (c) -27° (the MMS event) ($Z_X \sim 1.8 R_E$)
 - (d) 15° ($Z_X \sim -1.4 R_E$)

The white “X” denotes the subsolar X line location Z_X .

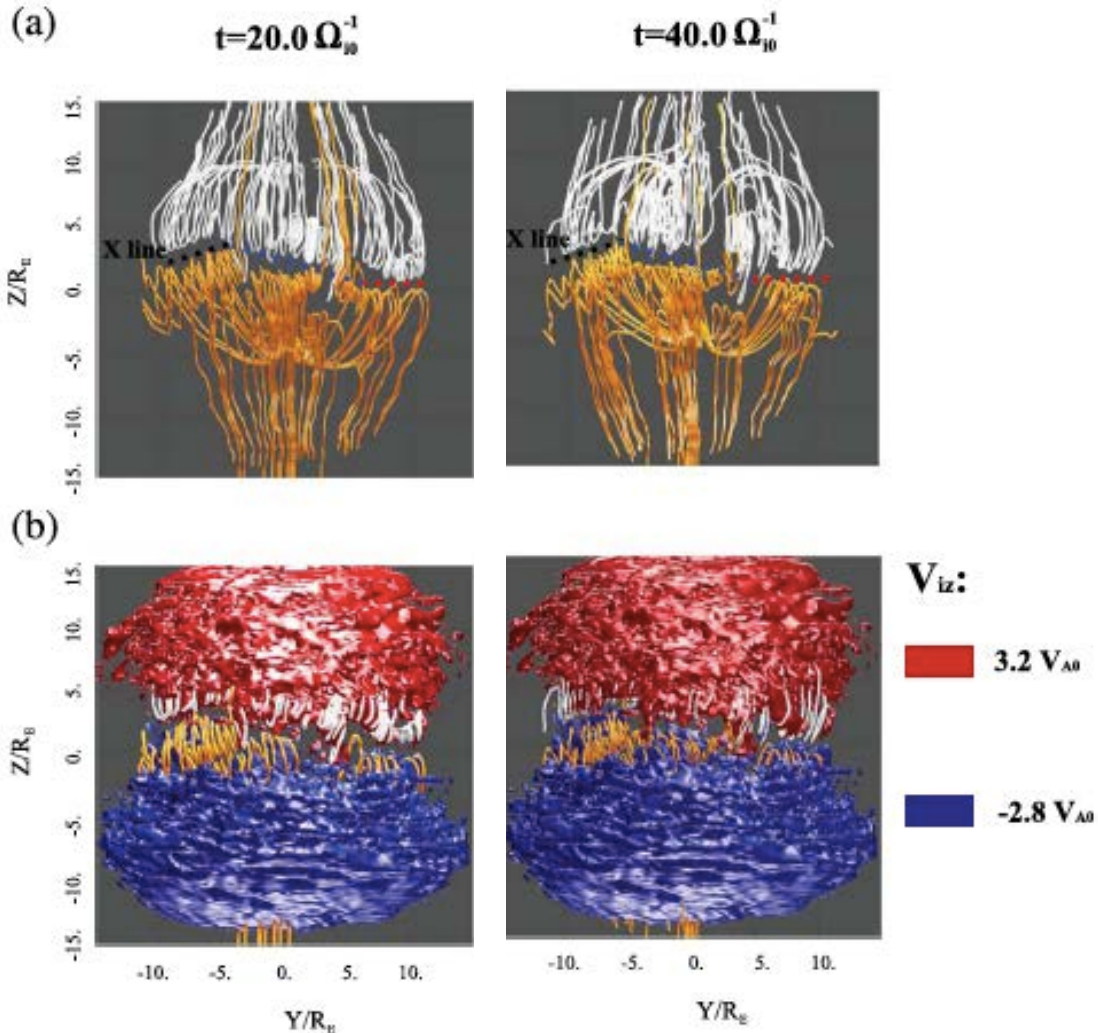
Simulation of the GEM Dayside Kinetic Challenge Event (18 Nov. 2015 Magnetopause Crossing)

-- Simplified purely southward IMF of 6nT, tailward dipole tilt of 27°, solar wind speed of 360km/s, and $M_A = 8.5$.



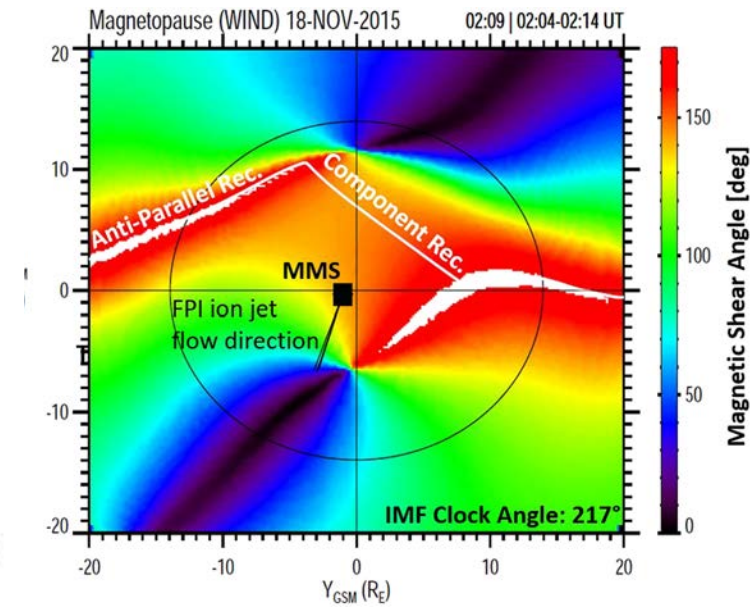
Comparison with MMS observation

Simulation



Guo et al. [2020]

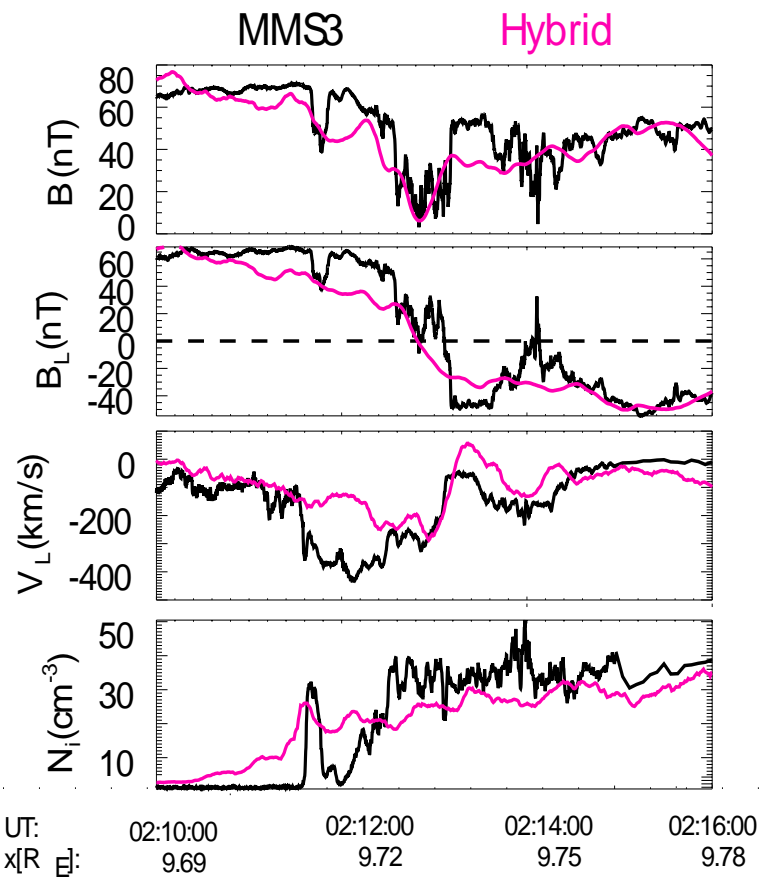
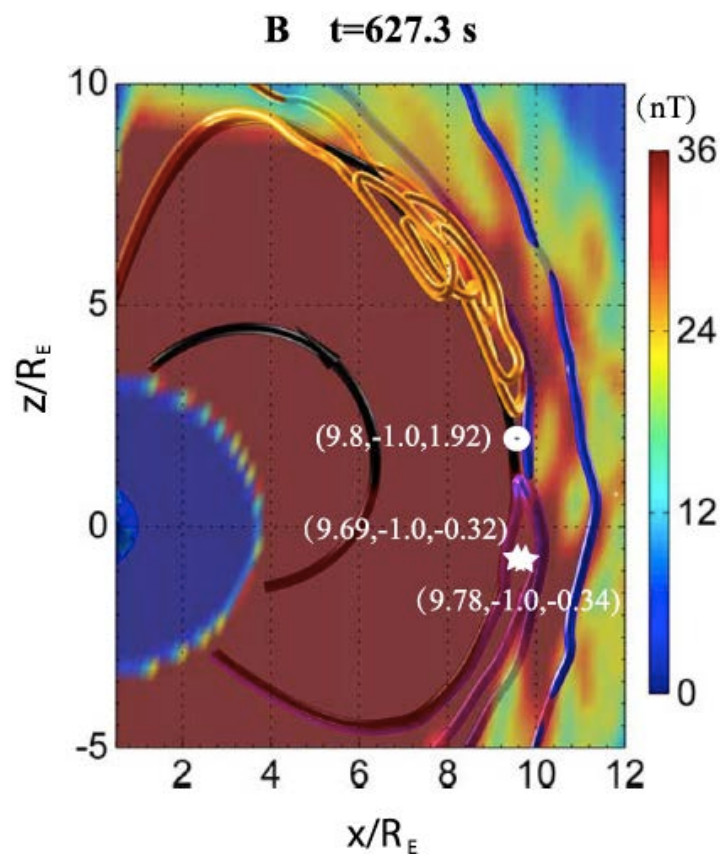
Observation



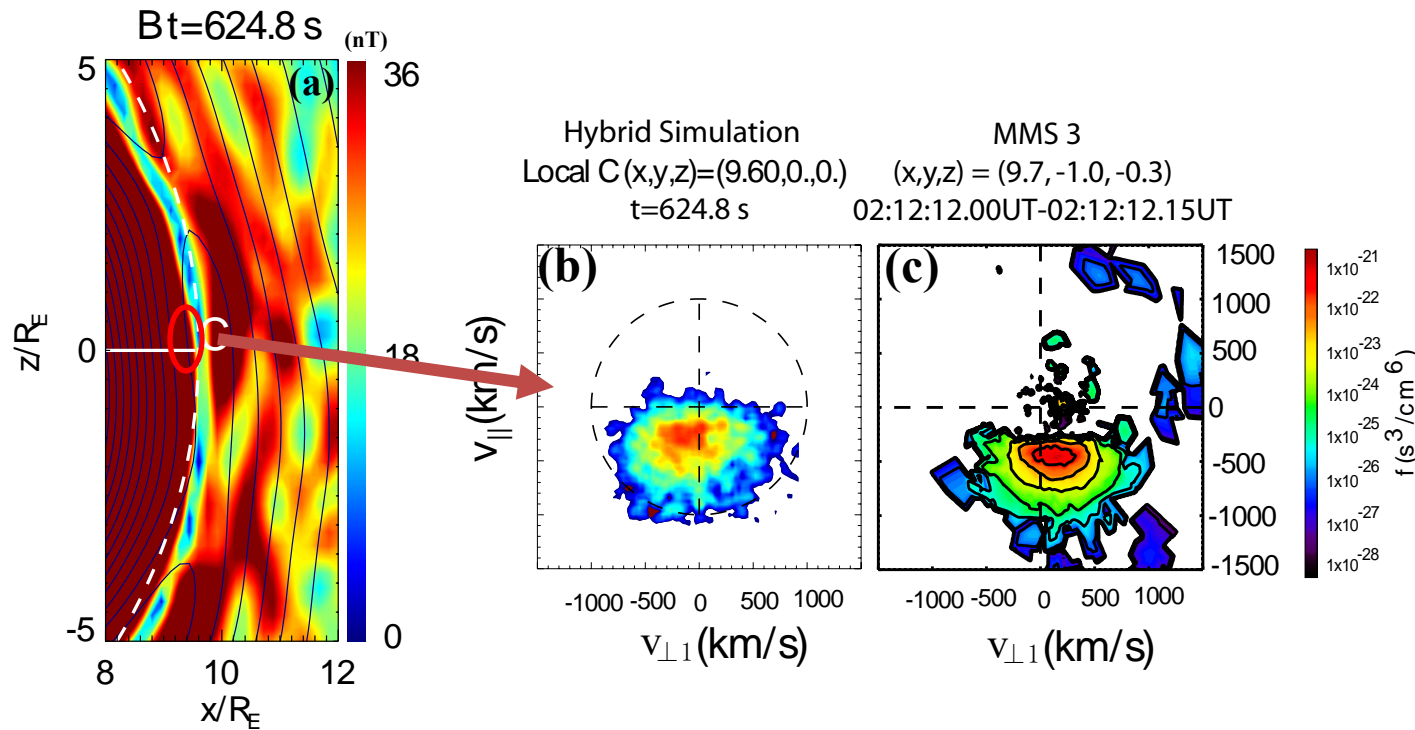
Trattner et al. [2020]

Predicted location of the dayside X-line based on the maximum magnetic shear model.

Comparison with MMS observation: structure of reconnection

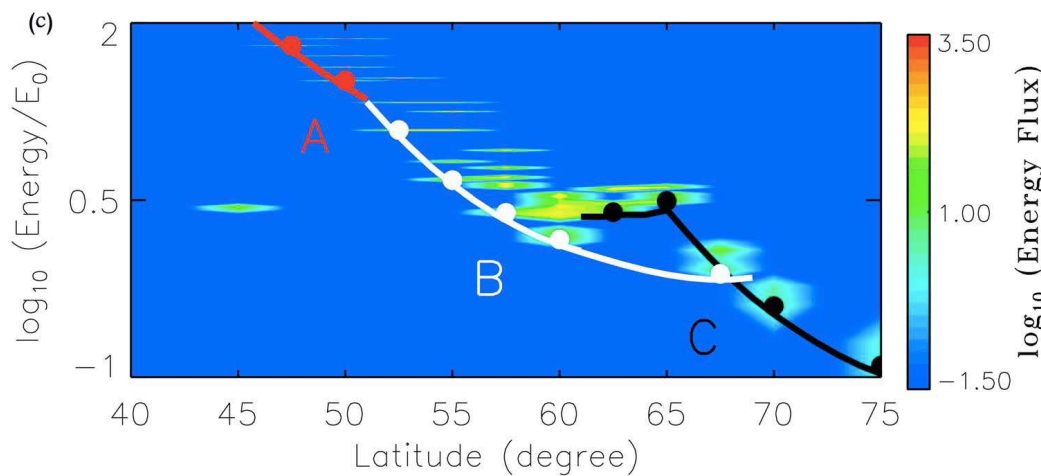


Comparison with MMS observation: D-shaped ion velocity distribution

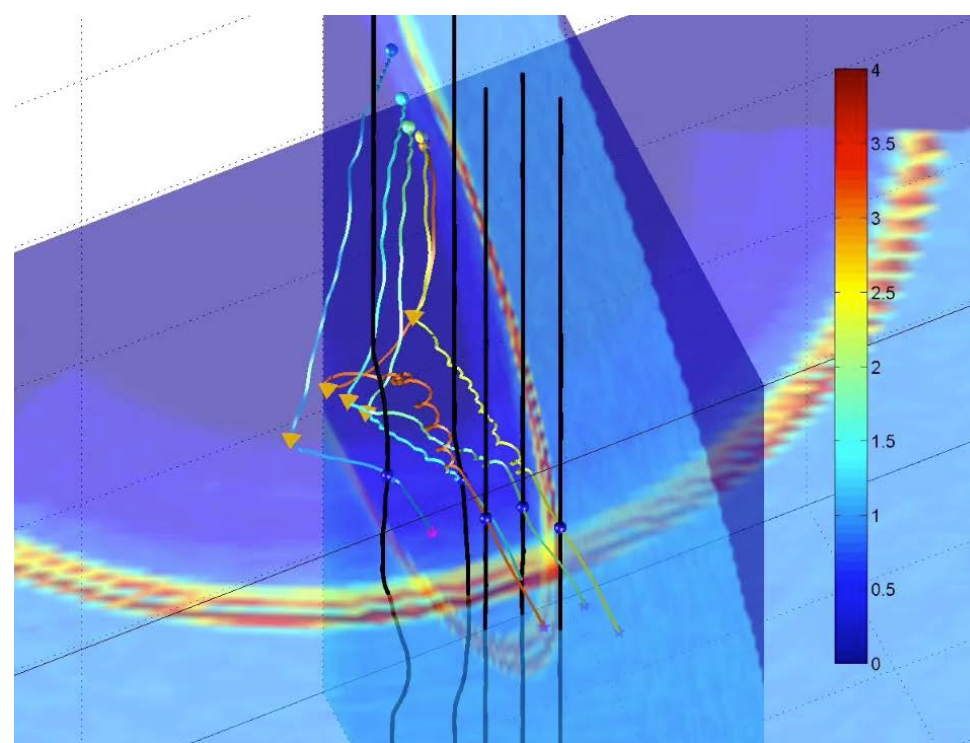
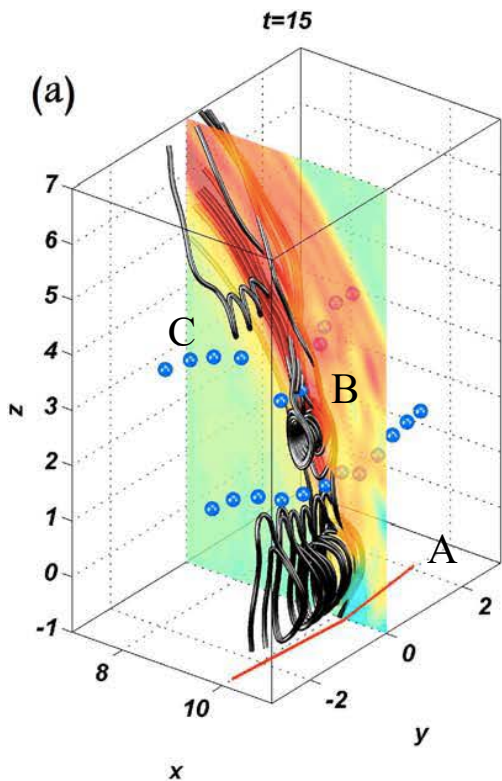


Tracking ion precipitation from magnetopause reconnection to the cusp

Tan et al. [2012]



Dispersive energy spectrum associated with time-dependent reconnection at multiple sites (A, B, and C) at the magnetopause.

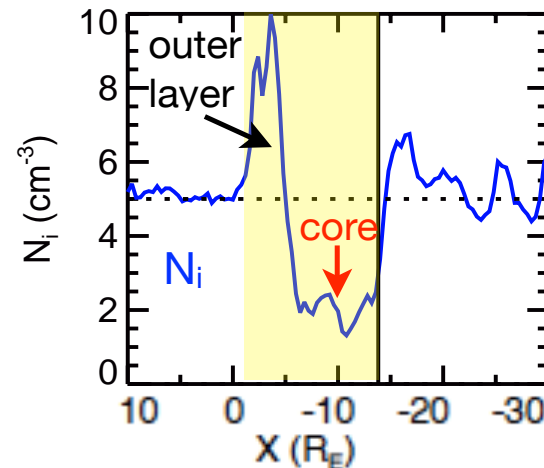
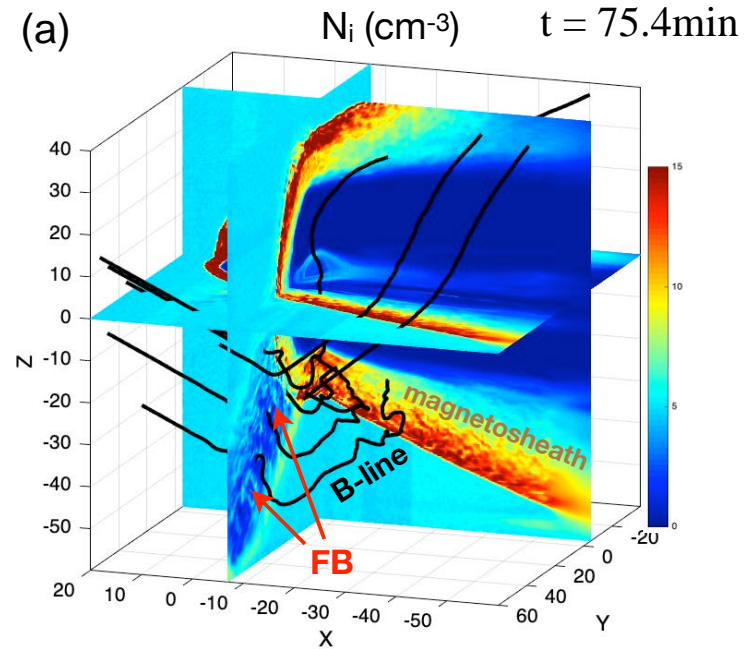
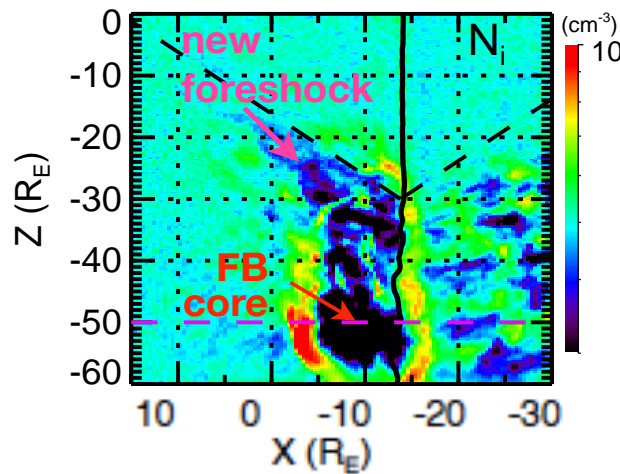


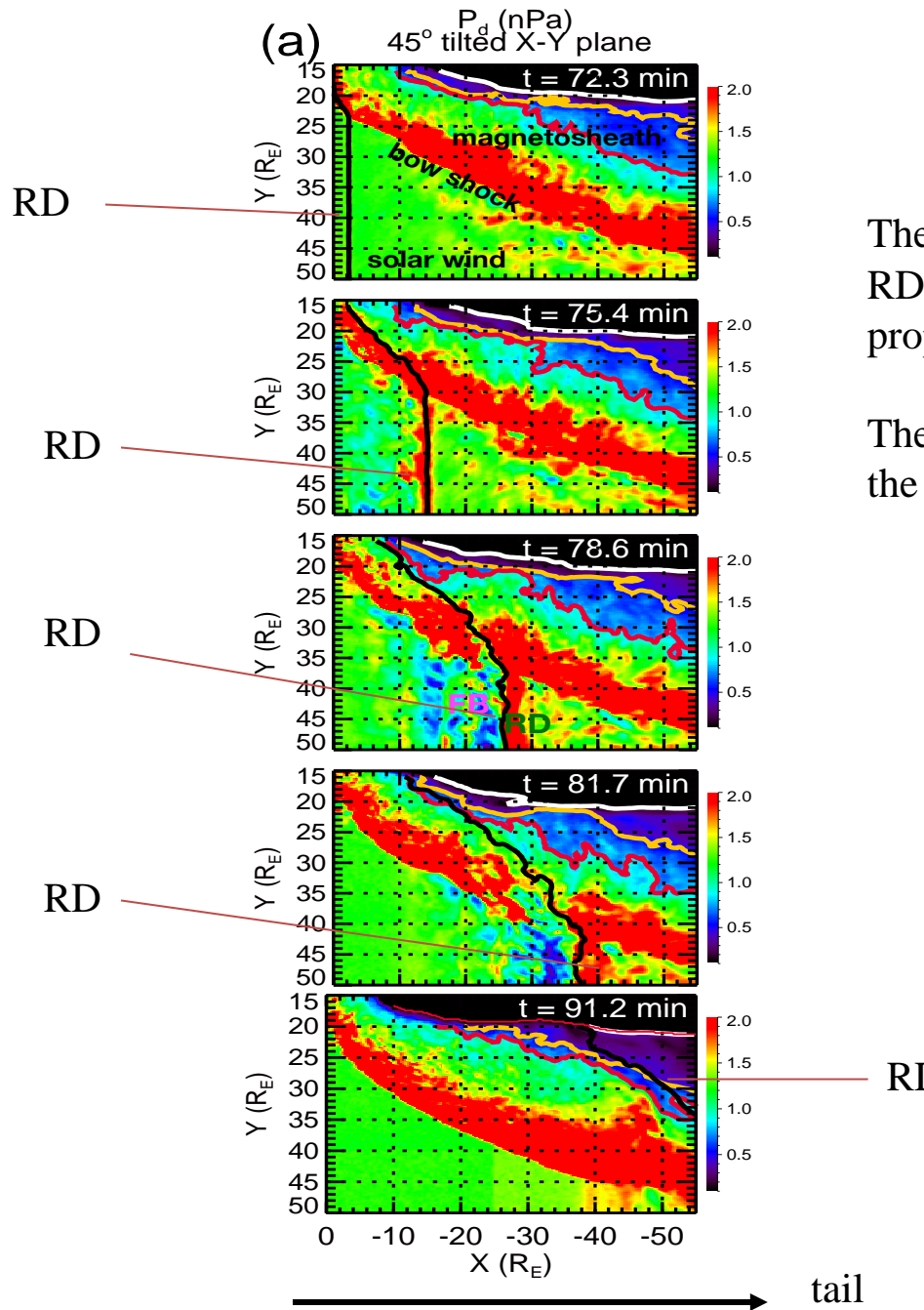
5. Results (3): propagation of dayside foreshock transients to the tail

Foreshock interaction with RD: foreshock bubble in the tail [Wang *et al.*, 2020].

Across RD: IMF rotates from $(2, 2, -2)$ nT on the anti-sunward side (downstream) of the RD to $(2, 2, 2)$ nT.

$t = 75.4\text{min}$, $y = 50R_E$





The foreshock transient expands around the RD-bow shock interaction region while propagating to the tail.

The foreshock bubble causes perturbations in the magnetosheath and on tail magnetopause.

6. Summary

3-D Global hybrid simulation, solving nonlinear physics from ion kinetic to global scales, shows:

1. Shear Alfvén waves/KAWs are generated in reconnection (consistent with local simulation in slab geometry) and play important roles in ion heating and anisotropic temperatures. The KAWs are present everywhere in the magnetotail, including the dipole-like magnetosphere. The Flow braking region in front of the ring current plays an important role in the flow of shear Alfvénic energy to the ionosphere.
2. On the global scale, the wave generation and ion heating are a much more involved process due to the nonuniformity and multiple boundaries.
3. In the simulation of a case of MMS magnetopause crossing of reconnection under a dipole tilt and a southward IMF, the near subsolar X line is tilted. The formation of multiple X lines, and thus flux ropes, begins from the generation of an X line above the equator. As the X line moves poleward, a new X line re-forms near the original location. The magnetopause reconnection is not in a steady state. The structure of reconnection, the global distribution of X lines, and the ion velocity distribution are consistent with the observation.
4. In the simulation of transient structures in the quasi-parallel shock, a foreshock bubble is generated upstream of an RD as it interacts with the bow shock. The transient structure propagates to the tail with the RD and grows with time/distance, causing pressure pulses in the magnetosheath and on the magnetopause.